WHOLE ORGAN CULTURE MODEL FOR SODIUM PENTABORATE PENTAHYDRATE TREATMENT OF PROSTATE CANCER

by
Mehmet Ali Karaca

Submitted to Graduate School of Natural and Applied Sciences
in Partial Fulfillment of the Requirements
for the Degree of Master of Science in
Biotechnology

Yeditepe University
2019

WHOLE ORGAN CULTURE MODEL FOR SODIUM PENTABORATE PENTAHYDRATE TREATMENT OF PROSTATE CANCER

APPROVED BY:

Assist. Prof. Dr. Hüseyin Çimen .....
(Thesis Supervisor)
(Yeditepe University)

Assoc. Prof. Dr. Ali Özhan Aytekin .....
(Yeditepe University)

Assoc. Prof. Dr. Gürler Akpınar .....
(Kocaeli University)

DATE OF APPROVAL: ..../..../2019

ACKNOWLEDGEMENTS

I would like to thank my supervisor, Assist. Prof. Huseyin CIMEN for his continuous support and motivation during my graduate study. I also want to thank YediPROT members and molecular biology, nanobiotechnology, regenerative biology, and molecular diagnostic groups for their help and support.

I would like to thank Nanobiotechnology Laboratory for SEM experiments and the Histology Laboratory in Faculty of Medicine for histology experiments.

ABSTRACT

WHOLE ORGAN CULTURE MODEL FOR SODIUM PENTABORATE PENTAHYDRATE TREATMENT OF PROSTATE CANCER

Drug discovery and toxicity experiments have been performed via different cell culture models for several decades. Two dimensional (2D) cell culture model has been widely used as an *in vitro* technique to test drugs. However, monolayer cell culture (2D) is not suitable for metastatic colonization and evaluation of drug resistance in cancer cells *in vitro*. Extracellular matrix(ECM) has essential roles in angiogenesis, particularly in cancer cell invasion. Construction of *in vitro* cell culture models which mimic *in vivo* is the ideal way to solve early drug discovery issues. Acellular matrices which contain ECM components are used in 3D cell culture models in order to provide *in vivo* cellular phenotype and cell-matrix interactions.

Energy metabolism in cancerous cell plays crucial roles in their growth, survival, proliferation, and long term maintenance. Sirtuins, known as NAD^+-dependent deacetylases or ADP ribosyltransferases, regulate cell survival and change cellular energy state in cancerous cell. Protein acetylation, one of the many post-translational modification, is regulated by sirtuins in order to modulate energy-related metabolic pathways. Boron-dependent compounds have been used for the inhibition of prostate cancer proliferation in a dose-dependent manner. In addition, boric acid was also shown to interact with NAD^+, which might affect NAD^+/NADH ratio regulating sirtuin activity and cellular energy state. In this study, organoid cell culture model was constructed to examine the effect of sodium borate (NaB) on healthy, PNT1A, and cancer prostate cells, DU-145, and PC-3.

ÖZET

PROSTAT KANSERİNDE SODYUM PENTABORAT PENTAHEDRAT UYGULAMASI İÇİN BÜTÜN ORGAN KÜLTÜR MODELİ

On yıllardır farklı hücre kültür modelleriyle ile ilaç keşif ve toksik etki deneyleri gerçekleştirmektedir. 2 boyutlu *in vitro* hücre kültür modelli yaygın şekilde ilaçların test edilmesinde kullanılmaktadır. Ancak, tek katmanlı (2B) hücre kültürü *in vitro*'da kanser hücrelerinin metastatik kolonizasyon ve ilaca karşı gösterdiği direncinin değerlendirilmesinde uygun değildir. Ekstraselluler matris angiogenesis ve özellikle kanser hücre invazyonunda dikkate değer rolü bulunmaktadır. *In vivo* koşullarını mimik eden *in vitro* hücre kültür modellerinin oluşturulması erken ilaç keşif sorunlarının çözülmesinde ideal bir yoldur. 3B hücre kültür modellerinde kullanılan ve ECM birleşenleri içeren ve hücresiz matrisler *in vivo* hücre fenotiplerinin mimik edilmesini ve hücre matris etkileşimini sağlamaktadır.

Kanser hücrelerindeki hücresel enerji metabolizması kanser hücrelerinin büyümesinde, hayatta kalmasında, çoğalmasında ve uzun süreli korunumunda temel rol oynamaktadır. Kanser hücrelerinde NAD^+ bağımlı deasetilazlar yada ADP riboziltranferazlar olarak bilinen sirtuinler hücrenin hayatta kalmasını ve hücresel enerji değişimlerini düzenlemektedir. Bir yazılım sonrası translasyon olarak bilinen protein asetilenmesi enerjiyle ilgili metabolic yolakların ayarlanması sirtuinler tarafından düzenlenmektedir. Boron bağımlı malzemeler prostat kanser büyümesinde doza bağımlı olarak inhibe etmesinde kullanılmaktadır. Borik asit ile NAD^+ molekülünün etkileşiminin gösterilmesi NAD^+/NADH oranını, sirtuin aktivitesini ve hücresel enerji durumunu etkileyebileceği düşünülmektedir. Bu çalışmada NaB'ın normal prostat hücresi ve kanser hücreleri PNT1A, DU145, ve PC3 üzerindeki etkileri incelenmektedir.

TABLE OF CONTENTS

LIST OF FIGURES

LIST OF TABLES

LIST OF SYMBOLS/ABBREVIATIONS

2D	2 dimensional
3D	3 dimensional
ADP	Adenosine Diphosphate
AMACR	Alpha-methly-acyl-CoA racemase
AR	Androgen Receptor
ATP	Adenosine Triphosphate
BNTC	Boron neutron capture therapy
Ca	Calcium
CD44	Cluster of differentiation 44 marker
CD57	Cluster of differentiation 57 marker
DLM	Decellularized liver matrix
DNA	Deoxyribonucleic acid
DPM	Decellularized prostate matrix
ECM	Extracellular matrix
FA	Formic acid
FASN	Fatty acid synthase
Mg	Magnesium
GLUT	Glucose transporter
NaBC1	Na+ -coupled borate transporter
BNTC	Boron neutron capture therapy
HIF-1 α	Hypoxia-inducible factor 1-alpha,
GLUT	Glucose transporter
H&E	Hematoxylin&Eosin
HA	Hydroxyapatite
HATs	Histone acetyltransferase
HIF-1 α	Hypoxia-inducible factor 1-alpha
KAT	Lysine acetyltransferase
M1PK	Adenosine Triphosphate
M2PK	M2 Pyruvate Kinase
Mg	Magnesium

mRNA	Messenger ribonucleic acid
MS	Mass spectrometry
Na^+	Sodium
NaBC1	Na^+-coupled borate transporter
NAD^+	Nicotinamide adenine dinucleotide
PDH	Pyruvate dehydrogenase
PGA	Poly-glycolic acid
PK	Pyruvate kinase
PLGA	Poly(lactic-co-glycolic) acid
PLLA	Poly L-lactic acid
PSA	Prostate Specific Antigen
PTMs	Post translational modification
RLM	Recellularized liver matrix
RNA	Ribonucleic acid
ROS	Reactive oxygen species
SEM	Surface electron microscope
SIRT	Sirtuin
TCA	Tricarboxylic acid
TCP	Tricalcium phosphate
TiO_2	Titanium dioxide

1. INTRODUCTION

1.1. PROSTATE CANCER

Prostate cancer is a second most frequent cancer type in men and fifth most common cause of cancer-related deaths in men worldwide. According to GLOBOCAN 2018, 1.3 million prostate cancer people were diagnosed and 359.000 of them died worldwide in 2018 [1]. Prostate anatomy was described by Niccolo Massa in 1536 and detailed by Andrea Vesaliu [2], [3]. Normal prostate organ locates and enrolls urethary below the bladder and its size is 4×3×3. Prostate gland's main function is secretions of prostate fluids by epithelial cells of prostate and the fluid makes up about one third of the total volume of semen by epithelial cells of prostate.

Prostate composed of three distinct cell types are distinguished according to functional significance, their morphological characteristics, and relevance carcinogenesis. One of them is secretory lumunen cell, which are differentiated androgen-dependent cells. Characterization of luminal cells is performed by their expressed androgen receptors which are cytokeratins 8 and 18 and the cell surface marker CD57 [4], [5], [6], [7]. The other major cell type is basal cells that are placed between underlying basement membrane and luminal cells. Unless basal cells have low levels of androgen receptors, they cannot produce prostatic secretory proteins. Basal cells express cytokeratins 5 and 14 as well as CD44 [4], [5], [6], [7]. Last prostatic epithelial cell type is neuroendocrine cell. Neuroendocrine cells are androgen independent cells. They spread through basal layer. They express chromogranin A, serotonin and various neuropeptides.

Prostate cancers develop slowly in prostate gland with uncontrolled development of prostate cells. Growing prostatic ducts are appearing with highly proliferated tissue. Cells which located in prostate stroma regulate cancer initiation and progression [8]. Transition state of normal prostate cells into proliferative inflammatory neoplasia (PIA) in region of epithelial cells which is one of the significant initiation mechanism for prostate cancer early state [9]. Prostate neoplasia which is often considered a pre-cancer is proceed by areas containing high grade of PIA and carcinoma at region of PIA [10]. On the other hand, lipid biosynthesis is

other mechanism which causes increase of PIA and invasive cancer. There are two enzyme which are α-methylacyl-coA-racemase (AMACR) and fatty acid synthase (FASN) responsible for increase of PIA.

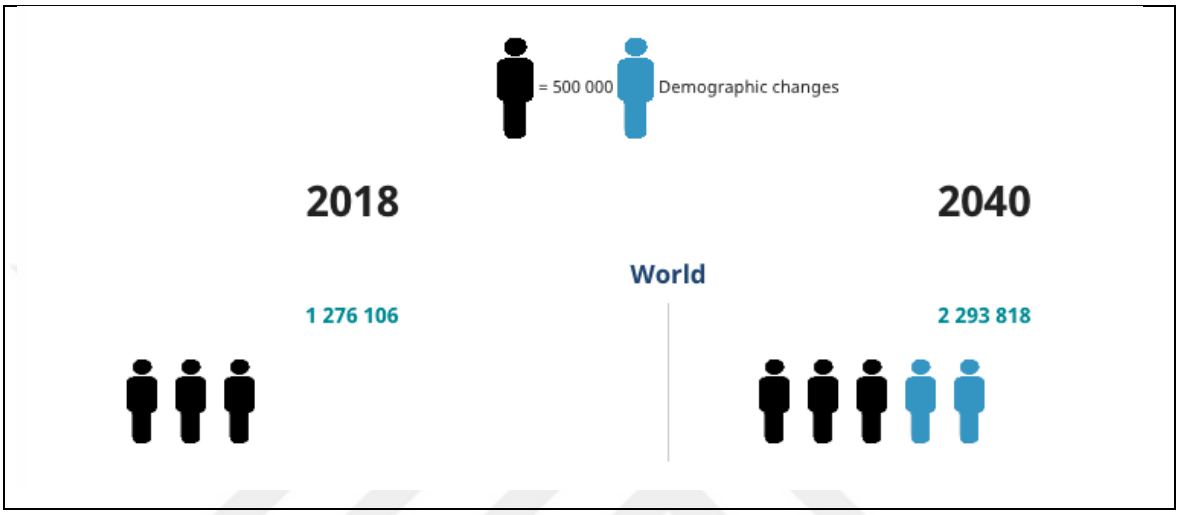

Figure 1.1. Predicted number of cancer cases from 2018 to 2040, prostate, males, all ages [1].

Aging is the other critical factor for early invasion carcinoma. Role of aging is related with telomerase activity which has a function on proliferation rate of prostatic epithelium. Study on telomerase dysfunction in prostate carcinogenesis causes accumulation of tumor promoting genomic alterations. Telomerase dysfunction forms disruptions of androgen receptors (AR) in prostate cancer cells and provides overcoming replicative senescence in prostate carcinoma cells [11]. Massive apoptosis of androgen dependent carcinoma cells causes tumor regression by androgen ablation therapy. Unfortunately, this therapy results highly aggressive and metastatic androgen independent prostate cancer. Generation of metastatic prostate cancer by androgen ablation therapy is developed by absence of expression of AR mRNA and protein.

1.2. CANCER MODELS FOR DRUG DISCOVERY STUDY

In vitro cancer models play crucial role for early steps of cancer drug assessment. Physiological relevant system of *in vitro* tumor models is important for progression and

treatment of cancer. Tumor models have been used to mimic metastatic cascade which is important for providing tumor cell proliferation, invasion, and cytotoxicity. ECM macromolecules which constitute 3D network regulate migration of tumor cell and acquired drug resistance in cancer cells [12], [13]. Combination of tissue engineering approaches with microfluidic technology is common methods which is used for rapid assessment of drug responses in cancer research. Understanding of cancer cell behavior in their local environment is main goal *in vitro* tumor models. Cancer models have also performed for drug discovery and toxicity studies before *in vivo* experiment for several decades. Monolayer cell culture model is widely used to test drug molecules *in vitro*.

1.2.1. Two-Dimensional (2D) Cell Culture Model

Monolayer cell culture models are still being used for prediction *in vivo* drug responses for cell-based screening and understanding molecular pathways. It provides high performance for functional tests and has low cost. Unfortunately, Monolayer cell culture does not contain tissue specific architecture and extracellular matrix which generates biophysical cues, and cell to cell and cell to matrix interactions. Absence of tissue specific architecture and extracellular matrix proteins causes failure to mimic natural environment of cancer [14]. Tumor mass is not represented in 2D cell culture models which does not provide cell to cell and cell to matrix interactions and coordinates cellular organizations, expression of genes and proteins, and drug resistance [15]. Conversely, isolated cell from healthy tissue subsequently adapted in 2D cell culture model and morphology of cells were altered. In short, 2D culture condition affect functional organization, phenotype, and signaling of cell. In addition, monolayer cell culture is applicable for only one type of cells. Tissue heterogeneity and tumor microenvironment, or niches, cannot be provided *in vitro* 2D cell culture models. Assessment of drug toxicity experiments which are performed in 2D cell culture models indicate low accuracy level because of the 2D cell cultures limitation. Limitation of 2D cell culture models reveals high amount of budget loss, labor loss, time loss, and redundant experimental animal. Best way to eliminate the difference between *in vivo* and *in vitro* experiments is construction of more realistic 3D cell culture models for *in vitro* drug discovery toxicity experiments and development process [16].

1.2.2. Three-Dimensional (3D) Cell Culture Technologies

Although 2D cell culture is a routinely used method for culturing of cells, it does not mimic anatomical structure or the physiological system inside the tissue. Absence of tissue architecture and ECM component limit investigation of 2D cell culture models. 3D cell culture methods can be mediator step of *in vivo* experiments for assessment of drug discovery. More realistic system for tissue-specific architecture which is supplied from 3D cell culture models can be designed with multidisciplinary manner. A different perspective in the process of construction of 3D cell culture models are used for the realization of the vascular network, matrix and porous structure, and ECM microenvironments. Spheroid microfabrication, organoid, hydrogel-based scaffolds, organ-on-chips, and 3D bioprinting on 3D cell culture which are common 3D cell culture technologies are more relevant systems for their application side.

1.2.2.1. Spheroids

Spheroids are made up of clusters of cells. In this model, cells form a 3D structure by attaching to each other in the absence of ECM structure. Spherical structures are more similar to solid tumors and provide oxygen, nutrient, metabolites, and soluble signals from the inside of spheroids to the outside of it [17]. Coculture models which are constituted with different cell types can also be formed as a spheroids model[18]. Formation of spheroid models can be performed with simple technique such as hanging drop. Application of drug testing and screening can be carried out with hanging drop plates. Different techniques which are rotating culture and concave plate methods also are used on modelling of solid tumor growth and metastasis studies [18], [19], [20]. A metastatic study which requires avascular tumor structure and micro metastases can be realized with spheroid modes which provide a physiological tumor [21]. Moreover, spheroid models are also applicable in high throughput screening for drug treatment as it is compared with hydrogel-based methods and organoids. Nevertheless, spheroid models do not contain native basement membrane proteins and carry out ECM-mediated cellular events.

1.2.2.2. Synthetic Scaffolds

Scaffolds in 3D cell cultures are a widely used construction for designing a tissue-specific structure and tissue modelling for *in vitro* studies. Scaffolds are basically classified into two groups which are synthetic and natural sourced scaffolds. Synthetic materials which enable to arrange their pores structure and alternate their surface chemistry have high mechanical properties, low biodegradability, and low biocompatibility [12], [13]. Synthetic scaffolds which are most commonly used in dental applications, orthopedic and bone tissue engineering applications are hydroxyapatite (HA), tri-calcium phosphate(TCP), and titanium dioxide (TiO2). Other synthetic polymers such as poly-l-lactic acid (PLLA), polyglycolic acid (PGA), and poly-dl-lactic-co-glycolic acid (PLGA) are used as a scaffold for *in vitro* studies.

1.2.2.3. Natural Scaffolds

Natural scaffolds promote excellent biocompatibility, low mechanical properties and provide surface attachment, adhesion, and growth of cells. Natural scaffolds are broadly classified into two groups: gel-based scaffolds and organoid culture. The most popular gel-based biomaterials are hydrogels and Matrigel.

Hydrogels are a composition of hydrophilic polymers which crosslinked to each other with covalent bonds. Hydrogel has an unique structure which can absorb a huge amount of water and also biological fluids. Swelling of hydrogel with biological fluid provides more suitable environment for cell survival. Presence of hydrophilic moieties develops backbone between the backbone of polymeric chains and carboxyl, amide, amino, and hydroxyl groups. Hydrogel has a similarity with natural extracellular matrix and carboxyl, amide, amino, and hydroxyl groups. Structural properties of hydrogels which are porosity, surface morphology, and size increase efficiency of cellular attachment, function, adhesion, and transplantation. Hydrogel has much more similar biomechanical and structural properties in soft tissue engineering application. Different cell types were tested for drug development and toxicity studies [20]. Common hydrogels in tissue engineering applications are chitosan and alginate-based hydrogels which have desirable biocompatibility.

Table 1.1. Characteristic properties of 3D cell culture models [22].

Characteristics	**Properties**
3D culture models	Animal models and organoid culture Spheroid based models Tissue sectioned culture Microcarriers Scaffold models
Advantages	Cell proliferation, number, viability monitoring Provide tissue specific morphology Characteristic differentiation of cells Reaction to stimuli Cell-cell interaction Tumor cell migration and invasion inside to surrounding tissue Polarization of cells inside tissue Mimic angiogenesis formation and Assessment of drug candidate Changes on protein profile and gene expression Cellular functioning inside tissue Physiological relevance system *In vivo* like environment
Limitation	Reproducibility of 3D models between batches Isolation of cells from matrixes Construction of 3D scaffolds Modification of 3D model volume Disallow to post culturing experiment Limited visualization inside scaffold Low performance and sensitivity of screening instrument process Optimization for drug discovery experiment Stabilization cell culture condition such as temperature and pH

The other popular gel-based biomaterial is the Matrigel which provides more *in vivo* like environment compared with synthetic sourced scaffold and hydrogels [23]. However,

compositions of Matrigel differ depending on lot-to-lot number which alters 3D cell culture experimental results. Biocompatibility study illustrated that 3D cell culture scaffold which is designed with fibrin, hyaluronic acid, chitosan, alginate, or silk fibrils has low biocompatibility properties compared that of Matrigel. Extracellular proteins such as collagen, fibronectin, and gelatin were included in Matrigel.

Organoids are animal sourced 3D scaffolds which contain extracellular membrane proteins, retain anatomical similarity [24]. Organoids are more similar models compared to other natural or synthetic biomaterial-based scaffolds for mimicking near *in vivo* system. Another natural scaffolds is Matrigel which assist complex mixture of ECM component and serve cell growth and derivation more efficient as compared to other 3D cell materials. Organoid provides simple and readable information about *in vitro* organ biology and drug discovery studies. Moreover, organoids models supply more similar *in vivo* like structure for cancer biology. However, complexity of ECM content is difficult to control variation of experiment results. The other limitation of organoid culture is absence of vascularization formation. Vascularization formation in organoids cell culture system could mimic *in vivo* like blood flow, oxygen and nutrient glucose supply.

1.2.3. Whole Organ Engineering

Study on organ transplantation is followed through on whole organ tissue engineering perspective. The first step of the whole organ engineering technology is decellularization which purified immunogenic materials and cellular components from a donor-derived tissue. Natural sourced scaffolds are common materials for organoid based 3D cell culture studies [25], [26], [27]. Construction of the decellularized matrix is based on purification of cellular component and immunogenic materials from native matrix. Decellularization process is carried out with infusion and draining cycles with different strategies. Decellularization techniques are basically classified into 4 groups which are physical, mechanical, enzymatic, and chemical. Physical methods are freeze/thaw, sonication, and mechanical agitation. These approaches are highly destructive for tissue morphological structure. Similarly, mechanical techniques is harshly affected on the morphological structure. The other technique is enzymatic decellularization. Enzymatic decellularization process is performed with different enzymes such as trypsin and endonucleases. Enzymatic process is effective for detachment

of cells from tissue. However, low penetration of enzymes solution inside tissue reveals decreasing of decellularization efficiency.

Chemical decellularization is more effective and suitable for preservation of tissue morphological structure. Different chemicals are applicable for decellularization process. Detergent based decellularization process is most commonly used techniques in chemical decellularization techniques. Ionic, nonionic, zwitterionic detergents are effectively used for removing the cell from the tissue by lysis of cell membrane and retaining of ECM components [28]. Detergent content, concentration, and sorting might be optimized for each tissue type. Each decellularization technique affects not only tissue morphology but also organ vascular and porous structure. Destructive vascular network affects recellularization efficiency, nutrient, and oxygen supply of tissue [29]. Decellularized matrix which contains collagen, elastin, fibronectin, laminin, and glycosaminoglycans differentiate according to each tissue types [30]. After recellularization of the matrix, proteins in retaining of the decellularized matrix play an essential role in intracellular protein expression [31]. Proteomics studies on organoids models are valuable approaches for organ biology and signification of extracellular matrix proteins for mimicking *in vivo* like physiological relevant system. Study on alteration of mRNA profile in the recellularized liver matrix by microarray data on days 8, 20, 28 illustrate that transcription of mRNA level is altered [27]. Designing of whole organ culture model is important for drug discovery and toxicity studies before *in vivo* researches.

1.3. 3D CELL CULTURE FOR DRUG DISCOVERY

3D cell culture has been used as an intermediate step before *in vivo* experiment for drug discovery. Limited information about cellular state inside the 3D matrix renders the utilization of the 3D cell culture methods debatable. Effect of drug on the cellular metabolism inside tissue is not detectable because of the cell heterogeneity inside the tissue. Complexity of tissue leads to *in vitro* 3D cell culture studies for simple identification of drug target mechanism intracellular level. Screening of cell morphology inside tissue is one of the important factors for assessment of drug effect. Limitation of microscopes which were used to resolve the structural information of specific molecule inside the cell is one of the disadvantages of 3D cell culture for drug discovery. Cells inside 3D cell culture or tissues could not be visualized because of the low signal penetration by microscope. Little

information about cellular state inside the 3D matrix renders the utilization of the 3D cell culture methods debatable. However, 3D cell culture models at proteomics level are powerful way for the detection of drug effect. Alteration of protein expression after treated with cancer drugs which are identified by proteomics analyzes predicate molecular mechanism of the drug. On the other hand, ECM targeted cancer drug is a novel therapeutic strategy for cancer therapy. Organoid based 3D cell culture which contains ECM proteins is important for the study of cancer drug [32]. Proteomics research on identification and characterization of ECM proteins are valuable for drug discovery studies and cellular mechanism.

1.4. BORON

Boron is semiconducting material and its atomic number is five. The density of Boron is 2.84 g/cm^3 and its atomic mass is 10.81 gram. 230 different types of boron are located in the world [33]. Turkey is a leading country for boron mineral reserves and 72.5 percent of of the boron in the world is located in the Turkey. Crystal structure of boron has similarity with diamond and it has physically similar toughness as a diamond.

Walnut, cherry, apple, bean, beet, pepper, and potatoes are boron rich nutrients. Boron is isolated from common elements that are oxidized form with boron found in nature. Generally, Boron is commonly found with Ca, Mg, Na metals. Boric acid which is most common type of boron has water soluble material, recycle into underground water and expand via surface and groundwater. In addition, boron is not only located in nutrients and water, but also placed in body fluid and tissue, has a role on different mechanism. Boron provides accumulation into bone and placed in heart, tissue, and lung. Boron can be rapidly absorbed from the gastrointestinal area in reference to pharm kinetic study. Low amount of boron converted into boric acid while absorbing mucosal surface depending on pH grade. Boric acid is a highly reactive molecule with amino, hydroxyl, and thiol groups. Boron which is low molecular weight and can react with organic compounds effect on biological functions [34]

Boron is an essential microelement for living organism nutrient supply. Boron affects on plant growth, cell wall structure, stress condition response, nitrogen metabolism. Boron is used in the medical area on different approaches indicates positive impacts such as bone and teeth cavitation, wound healing, anti-tumorigenic effect, antioxidant effect in blood enzyme

activity. Essential boron amount needed from adult individuals in a day shows an alteration between 1-13 mg. Amount of boron consumption in European countries is approximately 2-5 mg. It can reach 5,6 mg when an individual eats up with highly boron contain nutrients [33]. According to World Health Organization (WHO) statistics, boron intake in adult individuals is between the range of 1-13 mg. Boron specifically passes through from Na^+ coupled borate transporter (NaBC1) channel by passive diffusion [35], [36]. Yeast alcohol dehydrogenases can be inhibited by boron. The means of inhibiting dehydrogenases enzyme improve the growth of *Saccharomyces cerevisiae.*

Table 1.2. Application area and properties of Boron.

Application Area	**Properties**
Medical Industry	Physical Properties
Bone and Teeth Cultivation	Density 2.84g/cm3
Wound Healing	Atomic Weight: 10.81
Anti-tumorigenic Effect	Non-metallic in nature
Anti-oxidant Effect	Soft metal with low melting point
Antibiotic Agent	High electrical conductivity
Boron Neutron Capture Therapy	
Others	Chemical Properties
Glass Industry	Forms covalent compounds
Ceramic Industry	Electropositive metal
Agriculture	Unreactive in crystalline form
Metallurgy	
Nuclear Application	
Fuel Industry	

Boron is as a chemopreventative agent and applicable for different areas. Boron neutron capture therapy (BNTC) is one of the application area for healing of brain tumors with boron. Antimicrobial effect of boron is also be proved with different approaches for example; wound healing, anti-inflammatory effect, inhibition of cancer cell proliferation [37], [38]. Boron is soluble with hydrogen peroxidase which is excessively found in cancer cells. This

property gives chances to the application of boron in new cancer drug development. At the same time interaction of boron with reactive oxygen species increases the effect of cancer drugs [39], [40]. Moreover, cellular damage caused by oxidative stress is minimalized by increase of reduced glutathione with boron [41]. Rate of prostate cancer risk in geographical area where they have high amount of boron contained water and nutrient is low. These statistical results give an idea of boron therapy on the prevention and healing of prostate cancer. Moreover, boron effect on prostate cancer has been studied for so long. Study on increase of boron content in blood demonstrates a decrease of development of prostate cancer [42]. In case of other research on boron effect on androgen independent cell lines indicates that boron inhibits that androgen independent cell lines [43], [44], [43]. As the previous study on boron treatment in hepatocellular carcinoma shows that NaB based product can be designed for increasing treatment efficiency on hepatocellular carcinoma [45].

1.5. BORON EFFECT ON CELLULAR ENERGY METABOLISM

63 percent of cancer patient weight loss is detected in duration of cancer disease and 22 percent of them die of cachexy or other complications [46]. Glucose uptake in cancer tissue increases with low oxygen level in cellular level. Glucose is metabolized as a lactate with glucose uptake into cells via increasing of glucose level and this process occurs in presence of oxygen. HIF-1α which is basis of this process and stabile form in hypoxia environment is metabolized. Different research indicates that HIF-1α degraded in dominant oxygen environment [47]. Different mechanisms are discovered about enhancing of GLUT amount in cancer cell by HIF-1α [48], [49]. Glycolysis mechanism abnormally enhances in healthy cells compared with cancer cells and this increment is formed by uncontrolled working of three restricted enzymes [50]. The other mechanism for differentiation of glycolysis in cancer cell is indicated in pyruvate kinase step. Pyruvate kinase has a role on catalyze of glycolysis last control step and conservation of phosphophenol pyruvate to pyruvate. Even though dominant form of M1PK is in normal tissue, phosphorylation of M1 active site makes low level of M2PK become dominant in cancer cell. Conservation of pyruvate acetyl CoA decreases because of PK shows low activity in cancer cells. Thus, entrance of pyruvate conservation is prevented and formation amount of lactate is increased.

Limited study is performed about boron effect on cellular energy metabolism in literature. Boron interaction with NAD^+ molecule which effect on cellular energy metabolism has been shown by Kim and coworkers [51]. This interaction can be performed in cellular state and as a result of this interaction cellular energy metabolite in cellular energy pathways is affected. Boron and NAD^+ interaction directly changes many NAD^+ dependent mechanisms. One of the changes after NAD^+-borate complex formation is observed NAD^+ dependent acetylase or ADP ribosyltransferase which is known as a sirtuins. Sirtuins have role on cell survival and cellular energy metabolism. It has a main role on intracellular energy metabolism, growth of cancer cell, and cellular division. In recent research on cancer cells, cellular energy is recovered with cellular protein acetylation level as one of the post translational modifications. Acetylation is transfer of acetyl group to polypeptide chain of acetyl coenzyme A. 80-90 percent of proteins in human body can be acetylated from N-terminal. This reaction can be catalyzed by Nt-acetyltransferase. Acetyl transferase firstly discovered from acetylation of lysine side during histone regulated gene expression. For this reason, it is named as a histone acetyl transferase q(HATs) [52]. But lysine acetylation is not restricted with histone acetylation and named as a lysine acetyltransferase (KATs) [53]. This acetylation state is recyclable done with KDACs which is known as a lysine deacetylase. 7 different Sirtuins are identified in mammalian cells. While SIRT1, SIRT6 and SIRT7 were located in nucleus, SIRT2 was actively located in cytoplasm. SIRT 3, SIRT4 and SIRT5 are located in mitochondria and have effective role on metabolic process. Especially, SIRT3 has a role on different enzymatic activity.

1.6. MITOCHONDRIA

Mitochondrial defect in cancer cell is occurred with decreased oxygen uptake. This functional defect in mitochondria reveals undesired activity level of TCA cycle and electron transport system [54]. Pyruvate in healthy cells catalyzes with pyruvate dehydrogenases and forms an acetyl CoA molecule. Then Acetyl CoA molecule enters TCA cycle. PDH molecule which is active in dephosphorylated state was inhibited by phosphorylation state [54].Acetyl CoA molecules which were not metabolized is converted into lactate and metabolized. HIF-1α is used as a marker in some of the cancer types because of their role in this pathway [55]. Another reason for mitochondria disfunction is presence of reactive oxygen species which they inhibit complex 1 and complex 3 [56]. Mitochondrial energy, more than 90 percent, is

produced in hypoxia condition by oxidative phosphorylation and requirement of cellular energy is supplied with same pathway. Energy consumption by metabolic changes of cancer cells which increases glycolysis uptake plays crucial role for cancer researches. Lactate fermentation occurs in presences of mitochondria is called Warburg effect [57]. Moreover, increasing of glycolysis cycle in cancer cells shows that malignant phenotype of tumor formation. More than 20 of mitochondrial proteins are regulated by acetylation and deacetylation process which is one of the post translational modification. Acetylation of proteins were controlled by basic molecules and enzyme which were acetyl coenzyme (Ac-Coa), protein acetyltransferases, and NAD^+ dependent deacetylases. Synthesis of Ac-Coa which is occurred in cytoplasm and mitochondria deacetylated with SIRT1 and SIRT3 [58]. Different metabolic enzymes were located in mitochondria and regulate metabolism with acetylation. Acetylation of proteins were increases with concentration of Ac-CoA [59]. Protein deacetylation is performed with NAD^+ dependent deacetylases which is called sirtuins. NAD^+ dependent deacetylases have a main role on cellular stress responses and energy metabolism [60]. Seven different types of sirtuins (sirt1-7) have role on different cellular processes[61]. Alteration of NAD^+/NADH rate regulates amount of sirtuin activity. Increase of sirtuin content enhances deacetylation rate and activity of enzymes which have direct role on oxidative phosphorylation [62], [63], [64]. Mitochondria targeting drugs which were known as a mitochon induces cancer cell apoptosis [65]. Interaction of boron with NAD activates sirtuins which have a role on cancer cell energy metabolism and decreased resistance of cancer cell on apoptosis [45]

1.7. WARBURG EFFECT AND DRUG RESISTANCE

Respiration system of cells in well oxygenated environment operates glycolysis pathway and underutilizes their mitochondrial functioning [66]. Moreover, proliferation rate of cells is reduced and reveals the Warburg effect. Limitation of reactive oxygen species (ROS) production in Warburg effect promotes intracellular alkalization and activates HIF-1 which is one of the regulatory for disconnection of glycolysis from TCA cycle [67], [68]. Upregulation of membrane exchangers and downregulation of mitochondria control an alkaline pH inside cells. Basic cancer drugs could not be diffused inside cell which has a pH gradient each side of the cell membrane. Acidity which is outside of the cell promote positive regulation on functioning of efflux pumps which eject chemotherapy drug outside of the

cells [69]. Maintenance of an alkaline pH inside cancer cells is occurred by upregulation of membrane exchangers cells and induces glycolysis [70], [71], [72]. Efficiency of chemotherapy is very low because of the drug penetration into the cell.

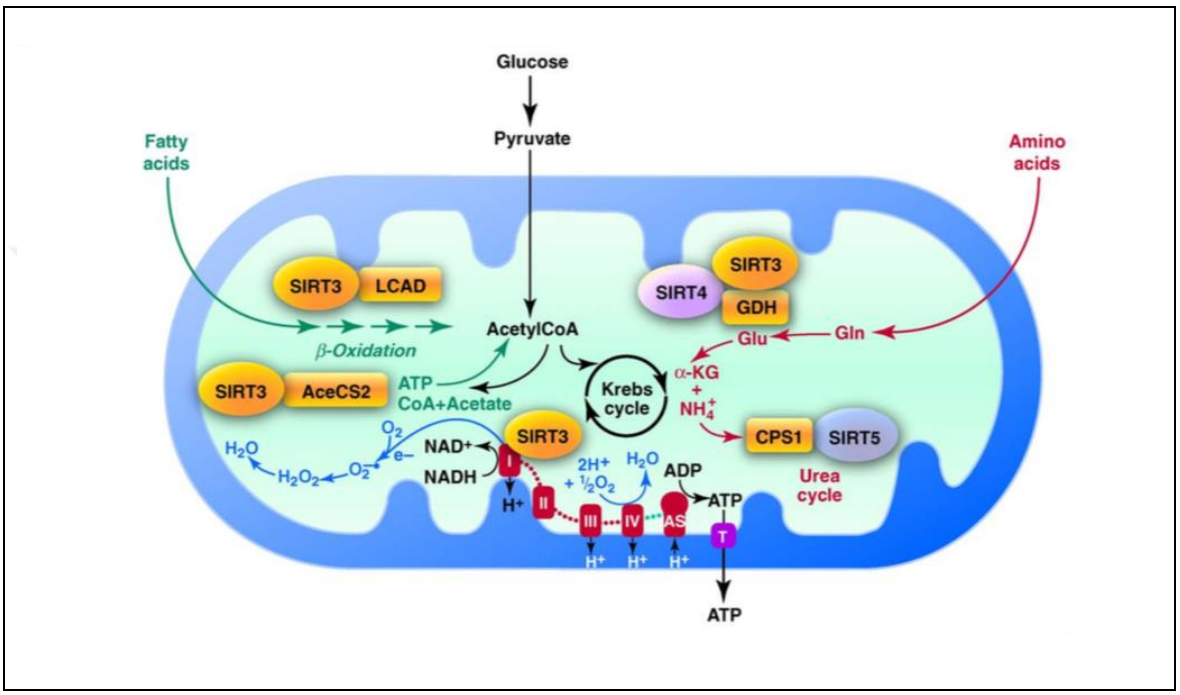

Figure 1.2. Mitochondrial sirtuins and metabolism [73]. Metabolization reaction of fatty acids, amino acids, and glucose is taken place inside mitochondria. Sirtuins organize cellular energy level. I–IV; red: electron transport complexes, AS; red: ATP synthase, AceCS2: acetyl-CoA synthetase 2, GDH: glutamate dehydrogenase, LCAD: long-chain acyl-CoA dehydrogenase, CPS1: carbamoyl phosphate synthetase 1.

However, assessment of metastatic colonization and evaluation of drug resistance cannot be performed in 2D cell culture models. Construction of realistic *in vitro* models by mimicking *in vivo* laboratory conditions provides tissue specific architecture and biochemical cues, cell-to-cell and cell-to-matrix interactions for assessment of metastatic colonization and evaluation of drug resistance [71], [74]. Low chemotherapy efficiency might be enhanced by molecules which target for glycolysis and oxidative phosphorylation. Molecules such as 3-bromopyruvate which play role on inhibition of glycolysis and OXPHOS and target to

mitochondria is called mitocons [75], [76], [77]. Inhibition of energy production in cancer cell by mitocons could increase citrate concentration and efficiency of chemotherapy drug [78], [79].

1.8. AIM OF THIS STUDY

Aim of this study is the construction of *in vitro* whole organ model for the effect of sodium pentaborate pentahydrate (NaB) molecule on prostate cancer. We have optimized decellularization procedure by SDS-based perfusion of whole organ and obtained decellularized prostate matrix (DPM) that preserved morphological, tissue specific architecture, and vascular structure. Whole DPM of male white rams is recellularized *in vitro* by perfusion of PNT1A, DU145 or PC3 cells intravascularly with a syringe pump. Comparison between 2D and 3D cell culture models is performed and whole organ culture model is constructed with decellularized liver matrix (DLM) for assessment of NaB on prostate cancer.

2. MATERIALS AND METHODS

2.1. SAMPLE PREPARATION

Whole Prostate organs of 14 male white rams (4–6 months old) were taken from a local slaughterhouse, and set in phosphate buffer saline (GIBCO, Germany). Then, surrounding fat is gently separated from whole prostate organs.

2.2. PROSTATE DECELLULARIZATION

Frozen prostates in PBS were thawed at 4 °C. Prostate was washed with PBS through perfusion via torsion testicular artery at 2 ml/min for 3 hours. The following decellularization method was performed for rams prostate: perfusion with 0.01 percent of SDS for 1 hour, PBS for 1 hour, 0.01 percent of SDS for 1 hour, PBS for 1 hour. Then prostate was incubated in 0.01 percent of SDS for 24 hours and then 0.1 percent of SDS for 24 hours and with 0.2 percent of SDS for 120 hours on rocker at +4C. Then prostate was incubated in 0.2 percent of SDS and perfused with 0.5 percent of SDS for 3 hours. Subsequently, prostate was washed with distilled H_2O for 2 hours and with 1 percent of Triton X for 2 hours. At the end of the procedure decellularized prostate matrix were shaken in PBS overnight at 4 °C. Residual DNA/RNA content in solution was measured using Nanodrop Technology (Thermo Scientific Nanodrop 2000). Sterilization of DLM was performed with 0.1 percent of (v/v) Peracetic Acid and 4 percent of (v/v) ethanol in sterile PBS for 3 hours at 4 °C and then DLM were washed with PBS (2 percent of Penicillin-streptomycin, 10 μg/ml Gentamicin, and 2.5 μg/mL amphotericin B).

2.3. ANALYSIS OF VASCULAR NETWORK

To visualize the vascular network inside whole prostate organ after decellularization, trypan blue(mod./MULTICELL) is injected through torsion testicular artery of whole prostate DLM. Vascular leakage and intact vascular formation inside whole prostate organ is

analyzed. In addition, vascular disorder which resist to flowing of flow through vessels is tested.

2.4. CELL CULTURE

Normal(PNT1A) and cancer (DU145 and PC3) cell lines were used for recellularization of whole prostate and cultured in DMEM with high glucose (GIBCO, Germany) at 37^{o}C and supplement with 1 percent of penicillin-streptomycin and 0.1 percent of Amphotericin B (GIBCO) and fetal bovine serum (GIBCO).

2.5. RECELLULARIZATION OF DECELLULARIZED PROSTATE MATRIX

Torsion testicular artery of prostate DLM was connected to syringe pump (Kd scientific kds 100 Syringe Pump). 50 mL medium was introduced into DLM at 6 mL/min. For recellularization 60 million immortal prostate cells (DU145 and PC3) were perfused with high-glucose DMEM (GIBCO, Germany) during 10 min culture periods (20 percent of FBS, 1:100 diluted Homemade Matrigel (1 percent of gelatin, 5ug/mL fibronectin, 5 ug/mL collagen)). After a 30 min perfusion with medium, 89 percent of of 60 million viable prostate cells were infused at 10-min intervals inside whole prostate DLM.

2.6. DECELLULARIZATION OF LIVER MATRIX

Livers which were collected from mouse were thawed at 4 °C. Livers were incubated with PBS for 1 hour. The following decellularization procedure was performed for mouse livers: incubated with in dH_2O for 1 hour, 0.01 percent of SDS for 1 hour, PBS 1 hour, 0.01 percent of SDS for 24 hours, 1 percent of SDS for 24 hours. Then, liver was incubated in 2 percent of SDS for 3 hours and then washed with dH_2O for 15 min and with 1 percent of Triton X100 (Sigma) for 30 min. At the end of the procedure decellularized prostate matrix were shaken in PBS overnight at 4 °C. Same procedure which is described section 2.5 without Homemade Matrigel is applied for recellularization of liver matrix.

2.7. HISTOLOGY

Decellularized and native prostate tissue sample were cut into areas of 0.5 cm-1 cm and placed in 10 percent of formaldehyde for 48 hours at room temperature. Then samples were washed inside dH_2O, dehydrated with graded ethanol, embedded by using paraffin, and divided into 5 um thicknesses. Samples were deparaffinized and hydrated in graded alcohol series. Sections were dewaxed in xylene and rehydrated by using graded alcohol series. Tissue sections were stained with Harris's Hematoxylin and Eosin (H&E) (Bio-Optica, Italy). All sections were mounted with DPX (Bio-Optica, Italy) and cover slipped and observed using by LEICA CTR600 B.

2.8. SCANNING ELECTRON MICROSCOPY

Prostate tissue samples were fixed with 2.5 percent of glutaraldehyde solution (Sigma, Germany) and then dehydrated in an ethanol (30, 50, 70, and 90 percent). Then, each samples were coated by using 3.5 mm of gold-palladium (SCD 005 Sputter Coater, Baltec) and investigated with SEM (EVO 40, Carl ZEISS, Germany) at 5 kV to ascertain the efficiency of decellularization and recellularization procedure.

2.9. SODIUM PENTABORATE PENTAHYDRATE (NAB) TREATMENT

PNT1A, DU145, and PC3 cells and RLM with prostate cells in low-glucose (1g/L) DMEM (GIBCO) were treated with NaB (sodium pentaborate pentahydrate from Boren, Turkey) for 72 hours period. Lastly, serum starvation was applied to control and NaB treatment group for 24 hours.

2.10. PROTEIN EXTRACTION AND DIGESTION

Tissue samples(RPM, RLM, DCM, and Native Tissue) are minced into small pieces and then freeze-thawed. Protein extraction from recellularized tissue samples and cell pellets was performed with RIPA lysis buffer system (Santa Cruz Biotechnology, USA) which is contain 1 percent of (v/v) PMSF, 1 percent of (v/v) protease inhibitor (PI) cocktail, 1 percent of

(v/v) deacetylation inhibition cocktail, 1 percent of (v/v) 1 mM sodium orthovanadate (Santa Cruz Biotechnology). Protein concentrations of each samples were determined by comparison to the bovine serum albumin (BSA) standard curve with Pierce BCA Protein Assay Kit (Pierce Biotechnology, USA).

2.11. IMMUNOBLOTTING

Protein samples isolated from native tissue, decellularized tissue, and recellularized matrix was loaded onto 10 percent of SDS-polyacrylamide gel and run 90V for 40 minutes and 120V for 120 minutes. 20 μg protein samples for each sample were analyzed. Samples were transferred from SDS page to a polyvinylidene difluoride (PVDF) membrane. For to analyze acetylome profiling of sample, immunoblotting was performed with acetylated lysine monoclonal antibody (Cell Signalling, USA) at 1:2500 dilution, beta actin antibody (Cell Signaling, USA) at 1:5000 dilution, and heat-shock protein 60 (HSP60) mouse monoclonal antibody (Abcam, UK) at 1:5000 dilution. Normalization of relatively acetylation of recellularized matrix and whole cell lysate was calculated for to obtain relatively acetylation level. OXPHOS enzyme complexes were analyzed with Total OXPHOS Rodent antibody (Abcam, UK) and HSP60 antibody is used as a control (Cell Signaling) at 1:5000 dilutions. Secondary antibody for acetylation which is antirabbit lgG (Sigma-Aldrich, USA) was diluted at 1:5000 ratio and for GAPDH, HSP60, and OXPHOS profiling which is rabbit was diluted at 1:5000 dilution. Analyzing of each image was performed using BIO-RAD ChemiDoc XRS + Molecular Imager with Lab Software.

2.12. TRYPTIC DIGESTION PROTOCOL

Gel band were minced about 1mm×1mm pieces. Pieces of gel were incubated with 25 mM ammonium bicarbonate and then dried with acetonitrile. Samples were reduced in 10 mM DTT at 59 °C for 30 min and then dried with acetonitrile. Gel pieces were alkylated using 55 mM iodoacetamide in ammonium bicarbonate and incubated for 20 min in the dark. Then gel pieces were washed two times with 25 mM ammonium bicarbonate. Samples were chemically two times dried with acetonitrile and then procedure is followed by mechanically dried using centrifugation. 0.15 μg trypsin were added to each sample. Gel pieces were

incubated overnight at 37 ℃. Extracted peptide fraction was collected and transferred to new tube. 5 percent of Formic acid (FA) was loaded in each tubes to quench the digestion. For to isolate residual peptide, 0.1 percent of FA was added to the gel pieces and then incubated at 37 ℃ for 10 minutes. Gel pieces were sonicated for 10 min and centrifuged for 8 min at 13000 rpm. The supernatant was centrifuged using vacuum-centrifuge.

2.13. PROTEIN IDENTIFICATION WITH MASS SPECTROMETRY

System is set as a " Pre-concentration on to a Nano Column". Samples were separated with 75 µmI.D. x 15 cm, Acclaim PepMap RSLC C18, 2 µm, 100Å column (Mobile phase A: 100 percent of water + 0.1 Formic Acid, Mobile Phase B: 100 percent of Acetonitrile + 0.1 percent of Formic Acid, Loading solution: 95 percent of / 5 percent of (v/v), water/acetonitrile and 0.1 percent of TFA). Peptide samples were loaded on nano-liquid choromotography (Thermo Dionex™ UltiMate™ 3000 RSLCnan). Inflow was arranged 0.300 µl/min (The following solution gradient procedure was performed with from 5 to 40 percent of mobile phase B at 50^{th} min, 95 percent of at 55^{th} min, 5 percent of at 65^{th} min and conditioning during 10 minutes) and separated peptide samples were analyzed with high throughput Bruker Compact, MS, nanoESI-qTOF (CaptiveSpray NanoBooster-Electrospray-UHR-Quadrupole-Time-of-Flight). System interfaces were control by HyStar 3.2, MS is controlled by otofControl ver:3.3, and analyzes were converted with .mgf for Compass Data Analysis program. NCBInr and SwissProt data banks were accessed with Mascot 2.4.1 and this file was used for protein identification with Biotools 3.2 program.

3. RESULTS

3.1. WHOLE RAMS PROSTATE WERE ISOLATED FROM MALE WHITE RAM

Male white ram prostate which provides large volume and surface area for cell proliferation was used as a 3D cell culture model for *in vitro* cell culture study. Male white ram prostate organ was constituted from two main prostate gland, torsion testicular arteries, prostate glands, and urethra (Figure 3.1). Vascular anatomy of whole prostate is composed of torsion testicular arteries, capillaries, and urethra. Torsion testicular arteries which is upside of prostate organ feed into prostate capillaries and released from urethra channel.

3.2. SDS BASED DECELLULARIZATION PROCEDURE COMPLETELY REMOVE CELL AND CELLULAR COMPONENT FROM PROSTATE

In order to obtain decellularized and transparent whole organ, SDS based procedure was applied on whole prostate organ via torsion testicular arteries. Decellularization procedure was carried out with different SDS concentration gradually from lowest to highest. Efficiency of procedure was increased with diffusion of SDS from inside to out of tissue. Transparent view shows that decellularized scaffold was obtained after application of SDS-based procedure (Figure 3.2). Residual nuclear material inside decellularized matrix was measured by using NanoDrop (Thermo Scientific) and amount of residual DNA content was 9,25 ng per mg of dry weight.

3.3. VASCULAR TREE OF WHOLE PROSTATE ORGAN WAS OBSERVED

In order to analyze intact vascular structure no leaky of whole organ was performed. Trypan Blue Dye (Multicell) was applied via torsion testicular arteries and vascular tree were observed. There was no vascular leakage inside and the on surface of organ in different section of the whole prostate organ (Figure 3.3).

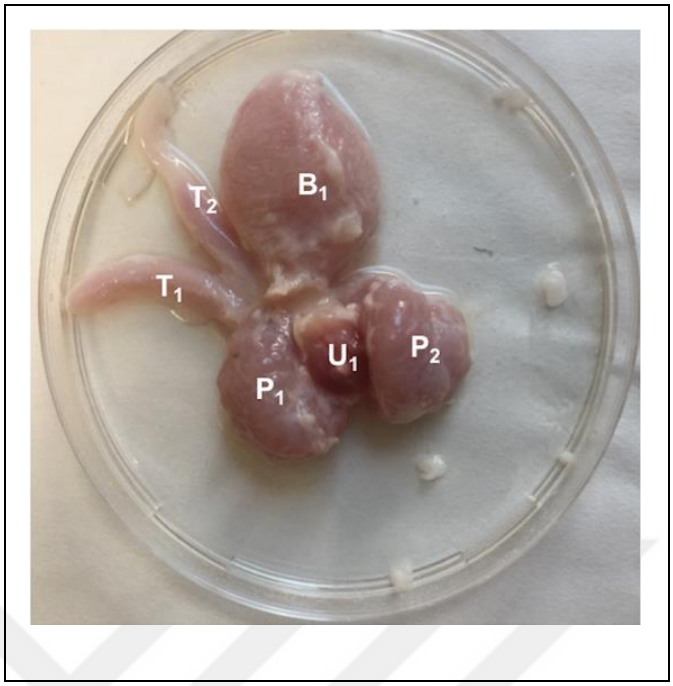

Figure 3.1. Anatomical structure of male white ram prostate is showed. (T_1, T_2) Torsion testicular arteries, (B_1) Bladder, (P_1, P_2) Prostate Glands, (U_1) Urethra.

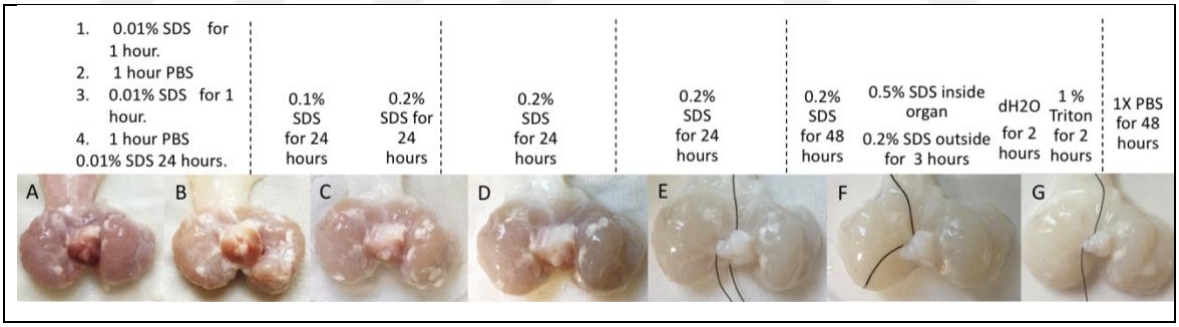

Figure 3.2. Figure illustrate decellularization process of prostate. Decellularization process is at day 0 (A), day 1 (B), day 2 (C), day 3 (D), day 5 (E), day 7 (F), day 8 (G). The prostate perfused through arterial vein as described above.

3.4. TISSUE MORPHOLOGY IS PRESERVED UPON SDS BASED PROTOCOL

Homogeneity of the decellularization process was controlled by histological assessment. One section of each decellularization matrix was dissected by scalpel cleavage. Specimens

were stained with Hematoxylin and Eosin (H&E) dyes. Histological investigation in prostate organ showed that general prostate architecture was preserved as demonstrated with native and decellularized prostate samples (Figure 3.4). Completed removal of cells and nuclei from ECM in all four sections was tested by Hematoxylin and Eosin (H&E) staining. Tissue architecture similarity was preserved when decellularized matrix compared with native matrix structure.

3.5. TISSUE ARCHITECTURE AND VASCULARIZATION IS PRESERVED

Scanning electron microscope was used to evaluate preservation of tissue architecture and vascularization. Maintenance of scaffold structure and vascular pores was observed. Fiber formation and pores for cellular attachment were constituted (Figure 3.5 (B), (E)). Additionally, arterioles were conserved during decellularization procedure (Figure 3.5 (A)). Arterioles, essential for nutrient and oxygen transportation to cells, was not been obstructed after recellularization and during cell proliferation (Figure 3.5. (C), (D)). Cellular profile and cellular extension is showed at Figure 3.5. (F). It shows that recellularization of decellularized prostate matrix is efficient where cells can easily be recognized.

3.6. DECELLULARIZED PROSTATE MATRIX CHANGES PROTEIN EXPRESSION OF PC3 CELL

SDS-PAGE experiment was performed for to analyze protein expression profile of recellularized prostate matrix. Recellularized prostate matrix with PC3 cells were cultured during 5 days. In figure 6, protein profile of PC3 cell inside decellularized prostate matrix was completely different when it compared with PC3 cell in monolayer cell culture. However, expected similar proteomic profile between recellularized prostate matrix and native tissue was not observed (Figure 3.6).

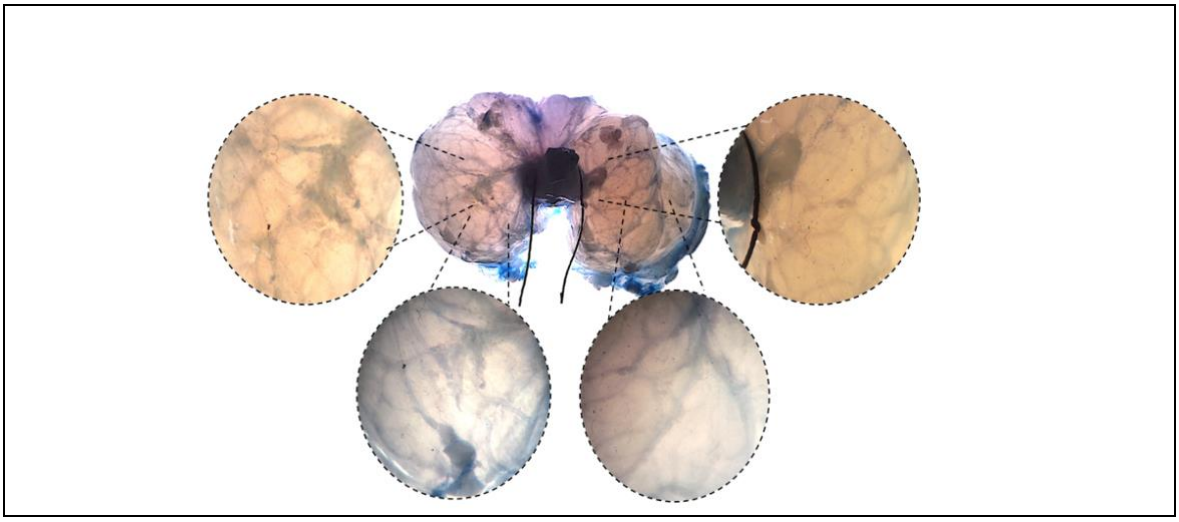

Figure 3.3. Decellularized whole prostate organ with vascular tree visible after perfusion with trypan blue dye.

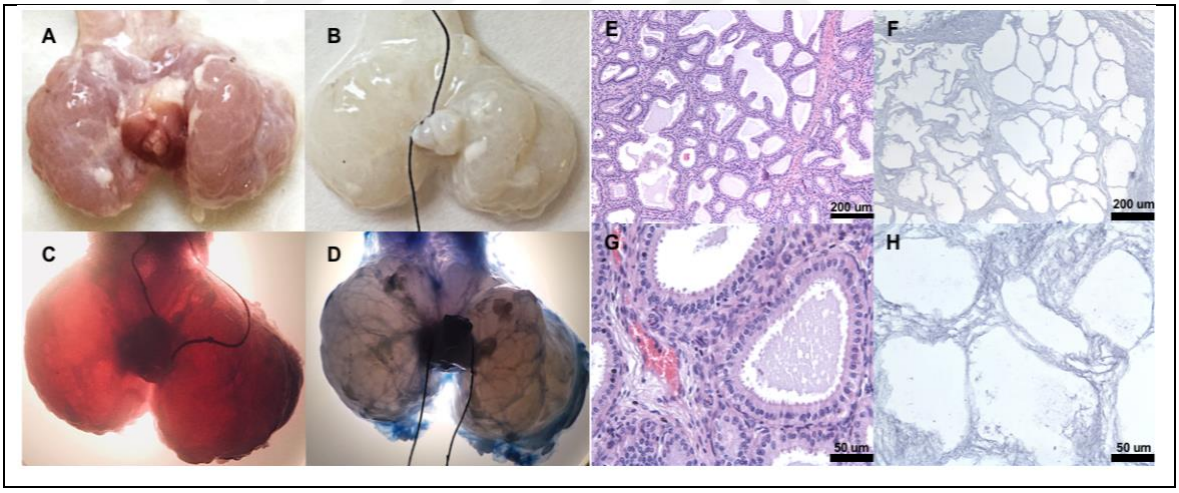

Figure 3.4. Representative images of whole male white rams prostate. (A) before (B) and after decellularization process, (C) after recellularization process. (D) Visulation of vascularization network with trypan blue dye. Histological analysis of ram prostate (E, G) comparison of native (F, H) decellularized prostate by Hematoxylin and Eosin (H&E).

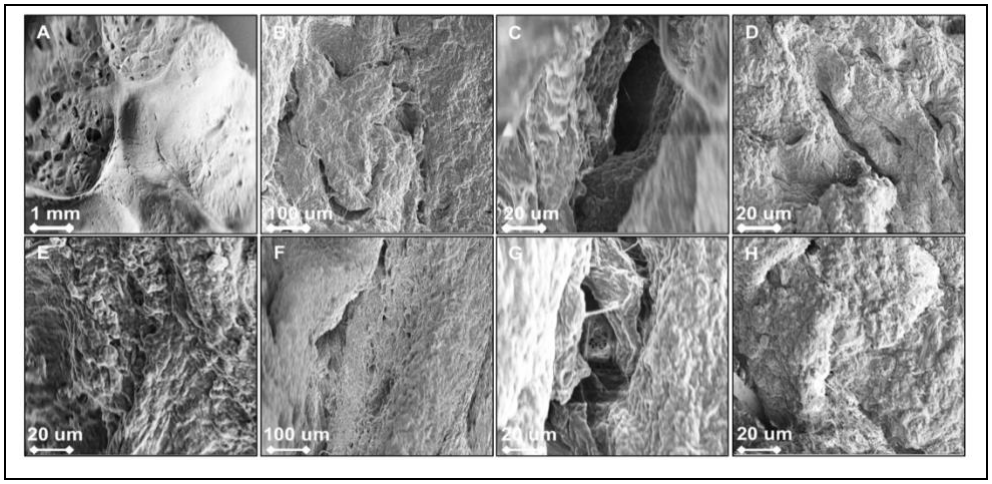

Figure 3.5. SEM images of prostate sample. Vascular formation of (A) native matrix, (B) decellularized matrix, (C, D) recellularized matrix is showing that preservation of vascular formation after decellularization and recellularization processes. SEM images of the (E) cellular structure of native matrix, (F, G) fiber formation of decellularization (H) absence of fiber formation is showed in recellularized matrix (H).

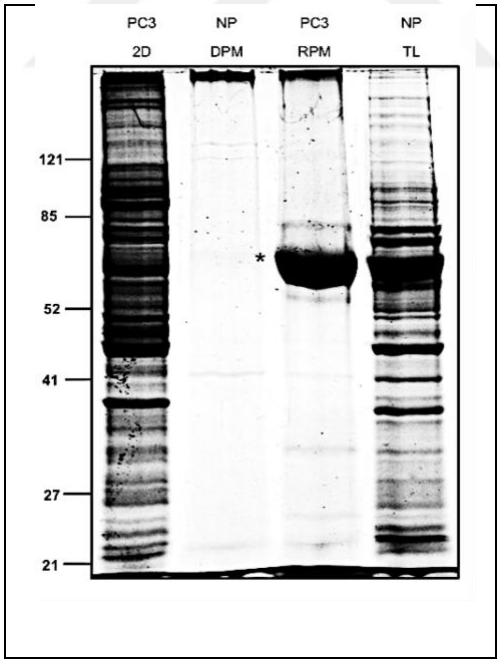

Figure 3.6. SDS-PAGE results displaying the changes in protein expression after recellularization. NP: Native Prostate, DPM: Decellularized Prostate Matrix, RPM: Recellularized Prostate Matrix, TL: Tissue Lysate. *: Fetuin A.

3.7. PENETRATION OF NUTRIENT AND OXYGEN INSIDE MATRIX DIDN'T CHANGE PROTEOMICS OF RECELLULARIZED PROSTATE MATRIX

Cellular proteome of recellularized prostate matrix was examined in the presence of different culture conditions. As a result of protein expression differences between monolayer and whole organ culture models is based on nutrient, oxygen and glucose uptake during the cell incubation. As a result of proteomics differences between recellularized prostate matrix and native matrix, effect of nutrient, oxygen and glucose uptake on PC3 cells inside whole prostate matrix was analyzed. Different samples were prepared which are; one of the prostate glands is cut at 1st day after recellularization, remaining section from cut area, and other prostate gland were incubated for 5 days (Figure 3.8, (A)). In figure 3.8, cutting side (CS) and whole section of recellularized matrix (WS) demonstrated same protein profile with recellularized prostate matrix. On the other hand, proteomes of between cell inside native matrix and native tissue were compared. Proteome of isolated whole cell lysate from native prostate tissue showed distinct protein bands compared to native prostate tissue. Most of the distinct protein bands were high molecular weight proteins, presumably extracellular matrix proteins. Similarly, distinct protein bands between protein profiles of isolated whole cell lysate from recellularized prostate matrix and of recellularized prostate matrix were also observed as high molecular weight region (Figure 3.8, (B)). The proteome differences between monolayer, whole organ, and native matrix might be resulted from protein mixture of ECM or differences of cell types between immortal cell lines and primary cell lines.

3.8. EXTRACELLULAR MATRIX PROTEIN CONTENT MODIFIES CELLULAR PROTEIN EXPRESSION

Gene expression of cells after recellularization was found to be differing 2, 15, and 28 [27]. We decided to examine the changes in proteins profiles of PC3 cells were tested on days 7, 15, and 21. Differences of gene expression were not observed in proteome level. Further, different immortal prostate cell lines which are normal cell (PNT1A), cancer cells (DU145, PC3) seeded inside the prostate matrix were analyzed. Significant differences was not observed any of these cell types.

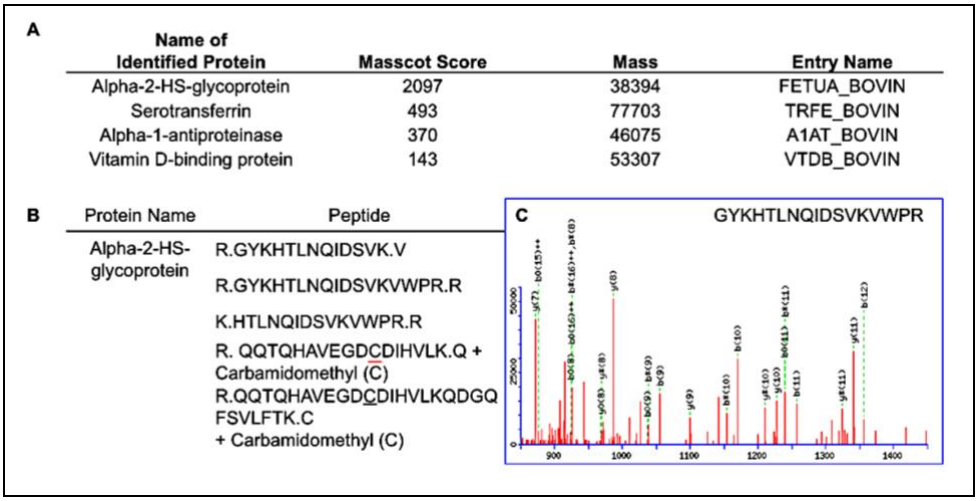

A

Name of Identified Protein	Masscot Score	Mass	Entry Name
Alpha-2-HS-glycoprotein	2097	38394	FETUA_BOVIN
Serotransferrin	493	77703	TRFE_BOVIN
Alpha-1-antiproteinase	370	46075	A1AT_BOVIN
Vitamin D-binding protein	143	53307	VTDB_BOVIN

B

Protein Name	Peptide
Alpha-2-HS-glycoprotein	R.GYKHTLNQIDSVK.V
	R.GYKHTLNQIDSVKVWPR.R
	K.HTLNQIDSVKVWPR.R
	R. QQTQHAVEGDCDIHVLK.Q + Carbamidomethyl (C)
	R.QQTQHAVEGDCDIHVLKQDGQ FSVLFTK.C + Carbamidomethyl (C)

Figure 3.7. MS identified Alpha-2-HS-glycoprotein. (A) Identification of proteins by In gel digestion method, and (B) peptides of Fetuin-A. (C) MS/MS result of alpha-2-HS-glycoprotein peptide.

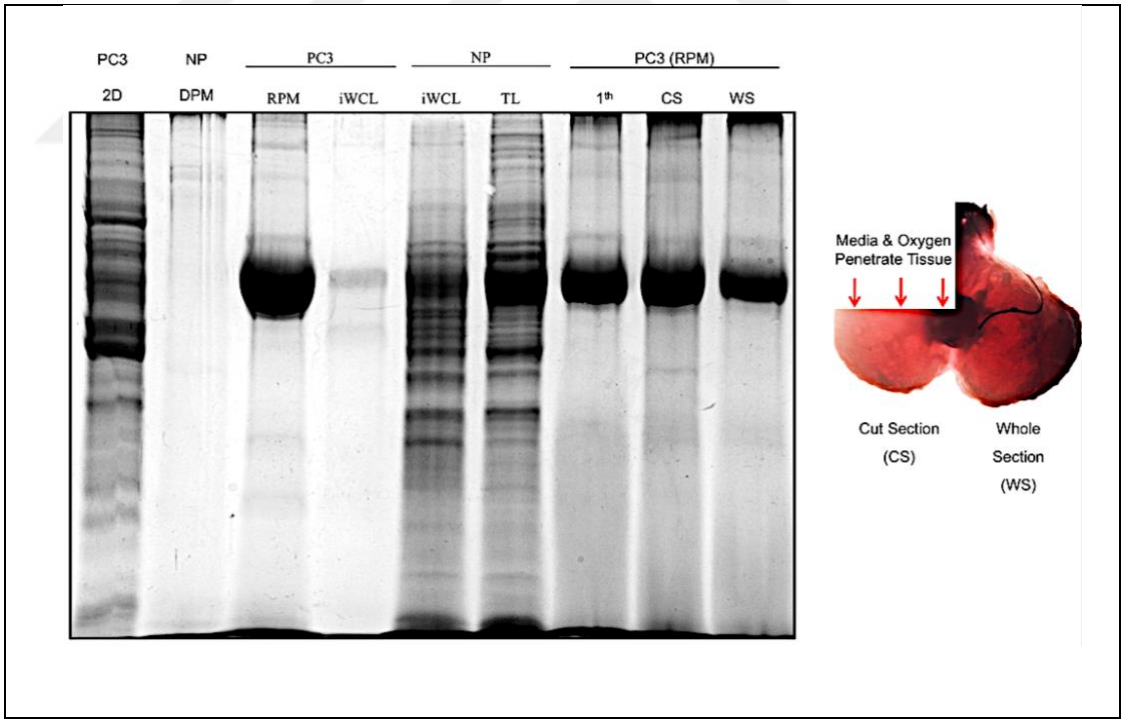

Figure 3.8. SDS-PAGE results displaying the changes in protein expression after examination of different culture conditions. 2D: Two dimensional, NP: Native Prostate, DPM: Decellularized Prostate Matrix, RPM: Recellularized Prostate Matrix, iWCL: isolated whole cell lysate, TL: Tissue Lysate, 1^{th}: First Day, CS: Cut Section, WS: Whole Section.

Then, home-made Matrigel, consisting of gelatin, fibronectin, and collagen with normal cell (PNT1A) was used to estimate effect of extracellular matrix on cellular protein expression. Cellular protein expression of PNT1A in Matrigel was completely different when it is compared to one from DPM. Band differences between home-made Matrigel sample and DPM samples suggested that content of extracellular matrix proteins definitely affects protein expression (Figure 3.9).

3.9. DIFFERENT ACELLULAR MATRIX CAN BE USED AS A 3D CELL CULTURE MODEL

Effect of different acellular matrixes on cellular protein expression was analyzed to optimize *in vitro* 3D cell culture model. Matrigel and liver, providing different extracellular matrix proteins were used as a 3D cell culture matrix. Liver matrix which supplies large surface area for cellular attachment and growth was applicable as an acellular scaffold for *in vitro* cell culture experiment. In figure 3.10. (A), protein profile of normal prostate cell in acellular liver scaffold displayed more similar proteomic profile to native matrix. Protein profile of RLM with prostate cells showed that acellular liver matrix with prostate cells can be used for *in vitro* 3D prostate cell culture study (Figure 3.10. (B)).

3.10. PROTEOME OF PROSTATE CELLS IN 2D CELL CULTURE AND 3D CELL CULTURE UPON NAB TREATMENT WERE ALTERED

SDS-PAGE experiment was performed for the analysis of sodium borate (NaB) treatment on 3D cell culture model. Acellular whole liver scaffold was recellularized with normal (PNT1A) and cancer (DU145) cell lines. Prostate cells in 2D and 3D cell culture was treated with 15 μg/ mL NaB. Protein expression profile was observed to be differing not only upon NaB treatment but also in 3D cell culture (Figure 3.11).

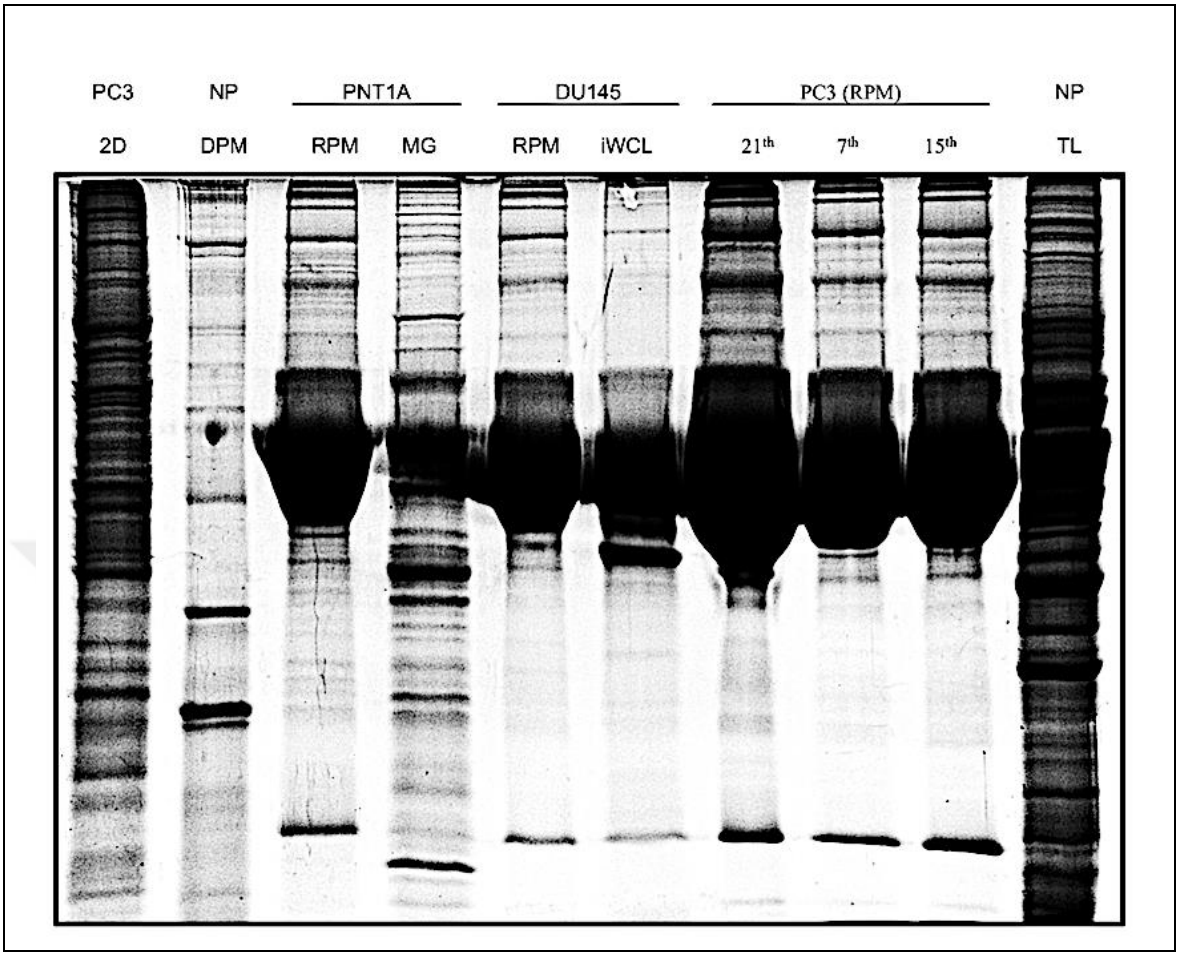

Figure 3.9. SDS-PAGE results displaying the changes in protein expression after analysis of different cell lines inside RPM. 2D: Two dimensional, NP: Native Prostate, DPM: Decellularized Prostate Matrix, RPM: Recellularized Prostate Matrix, MG: Matrigel iWCL: Isolated whole cell lysate, TL: Tissue Lysate, 7^{th}: First Day, 15^{th}: First Day, 21^{th}: First Day.

3.11. WHOLE CELL ACETYLOME AND EXPRESSION OF OXPHOS COMPLEXES OF PROSTATE CELLS IN 2D CELL CULTURE AND 3D CELL CULTURE UPON NAB WERE ALTERED

Deacetylase activity of whole cell lysates and recellularized prostate matrix were investigated in 2D cell culture and 3D cell culture model upon the NaB treatment. Whole cell acetylome was significantly altered not only between 2D and 3D cell culture models (Figure 3.12 (A)). Moreover, alteration of oxidative phosphorylation (oxphos) complexes between 2D and 3D was also observed, particularly in CIV and CI of DU145 cell lines (Figure 3.12 (B)).

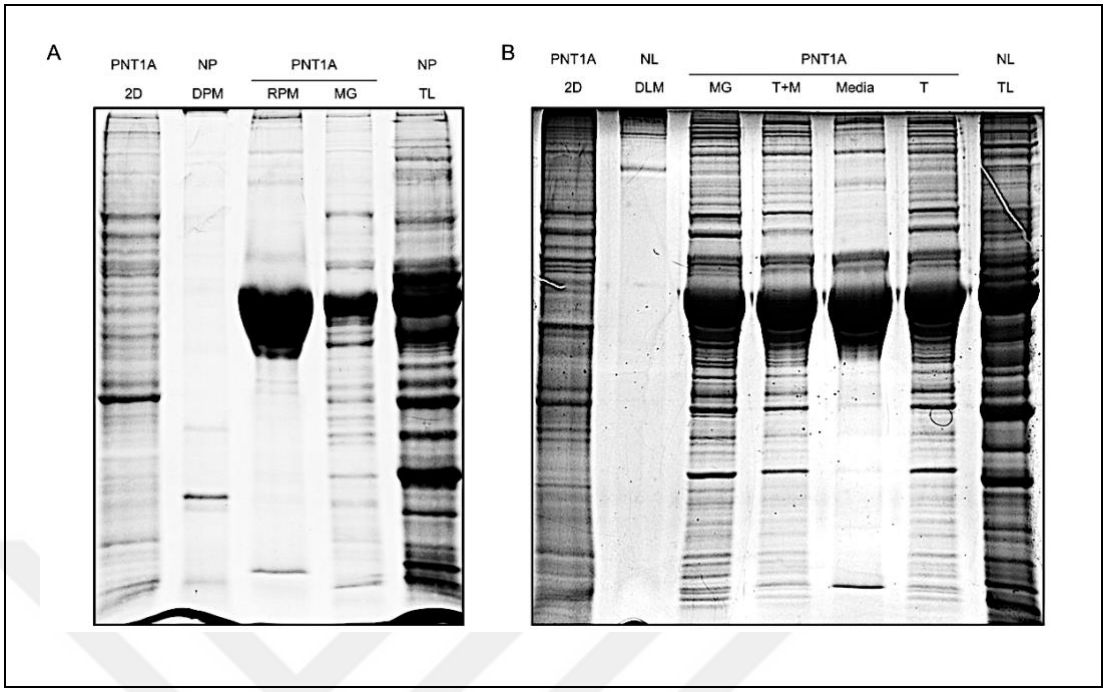

Figure 3.10. SDS-PAGE results displaying the changes in protein expression of PNT1A inside acellular liver and prostate matrix. 2D: Two dimensional, NP: Native Prostate, DPM: Decellularized Prostate Matrix, RPM: Recellularized Prostate Matrix, MG: Matrigel, NP: Native Prostate, TL: Tissue Lysate, T+M: Tissue and Matrigel, T: Tissue, NL: Native Liver

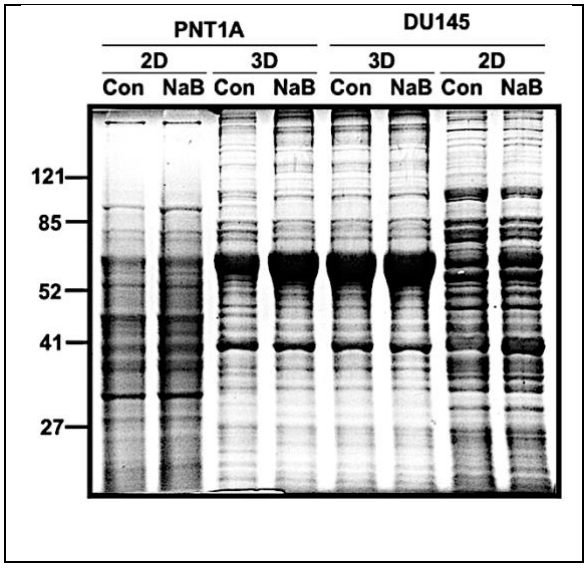

Figure 3.11. SDS-PAGE results displaying the changes in protein expression. 2D: Two dimensional, 3D: Three dimensional, Con: Control, NaB: Sodium Penta Borate Penta Hydrate.

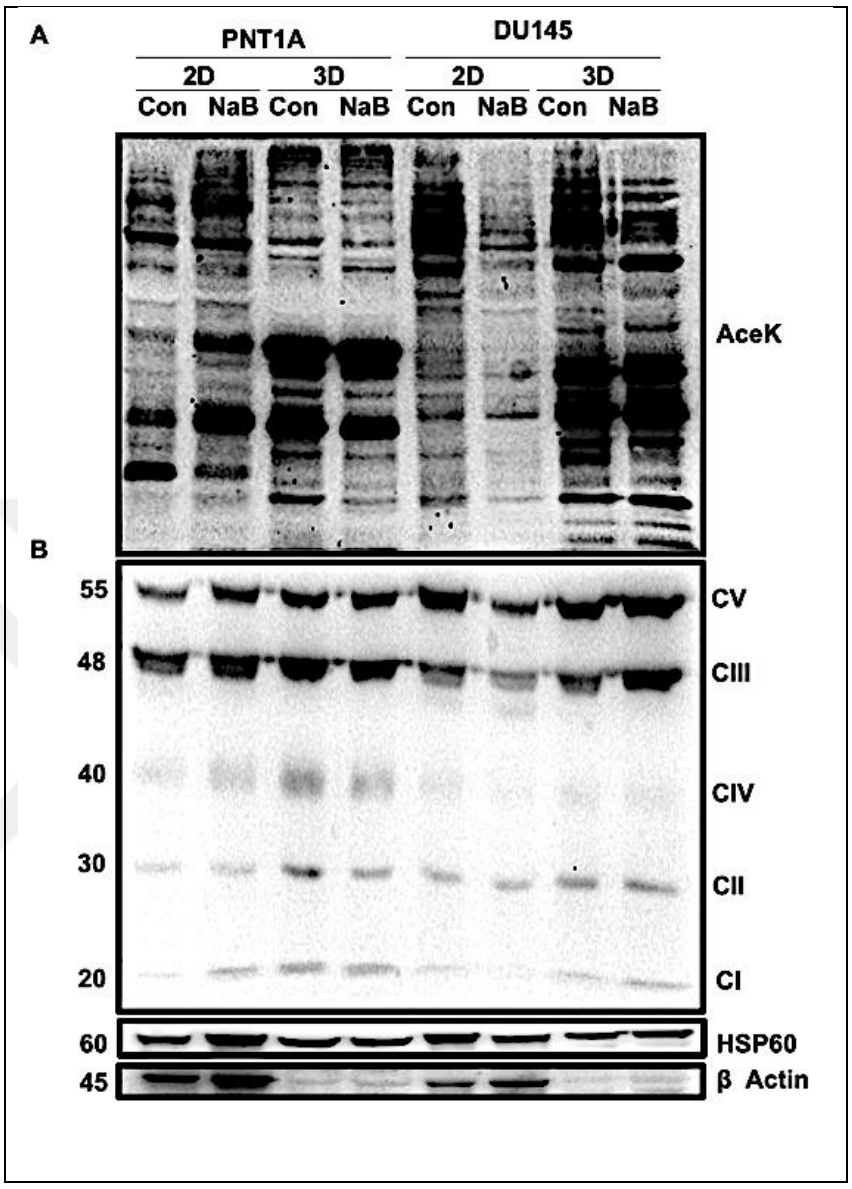

Figure 3.12. Immunoblotting experiment is performed. (A) cellular acetylome and (B) oxphos complexes between 2Dvs3D cell culture treated with NaB are analyzed. AceK: Acetylation, CV: ATP synthase, CIII: Cytochrome c oxidoreductase, CIV: Cytochrome c oxidase, CII: Succinate dehydrogenase.

4. DISCUSSION

In this study, preserved vascular structure inside acellular scaffold is examined for nutrient, glucose, and oxygen, access as well as drug by using is observed by using SDS-based method through vascular tree. The aim of this thesis was to investigate the differential effects of ECM proteins on cellular proteome and energy metabolism between 2D and 3D cell cultures upon NaB treatment. Our results showed that we successfully developed whole organ culture (acellular organoid) 3D models which were recellularized with immortal prostate cell lines and treated with NaB. NaB is used as a mitochon which targets on mitochondrial functions. Combination of NaB treatment with calorie restriction induces SIRT3 activity and restores mitochondrial function by reprogramming metabolism of HEP3B human HCC cells [62]. In this study, we hypothesized that extracellular protein content in 3D cell culture models might play an essential roles in energy metabolism, cellular acetylome, protein expression, and drug toxicity on cellular proteome.

NaB treatment, together with nutritional stress, alters intracellular NAD^+ level via chemical interaction. NAD/NADH ratio regulates sirtuin activity [80]. Alteration of NAD^+ pool in cell changes metabolic activity especially in energy metabolism. In addition, nutrient, oxygen, and glucose uptake by cells which are parts of energy production is completely different between 2D and 3D cell culture models. 3D system creates gradient of nutrient, oxygen, and glucose uptake from outside of 3D model to inside, which is similar to *in vivo* experiment model. Gradient access promotes nutrient stress inside 3D structure and causes heterogeneity of cancer cell and differentiation of cellular energy metabolism to the core of model structure. Additionally, drug toxicity studies in 2D cell culture models is indicate larger variability compared to 3D models. Similarly, efficiency of drugs on cancer cells is limited because of the drug resistance.

Penetration of drug molecules inside tissue is biggest gap in drug discovery studies for *in vivo* and *in vitro* models. Another one absence of vascularization formation and angiogenesis for assessment of candidate drugs to be used in cancer treatment. Gradient of nutrient, oxygen, and glucose is also present intravascular access *in vivo*. Given the vascular structure and 3D gradient to mimic *in vivo* like conditions, this would provide more possible way to eliminate additional candidate drug molecules which might not be effective in further tests. ECM is another regulatory factor for the migration of tumor cell and drug resistance in

cancer cells [81]. Cellular events such as differentiation, adhesion, proliferation, migration, and survival are related with ECM macromolecules such as proteins, chemokines, growth factors, and cytokines [82]. Drug molecules and diagnostic agents modify ECM protein expression and distribution. We have developed a practical *in vitro* whole prostate cancer model by using acellular scaffold for drug discovery studies. Decellularization method we established is a process providing successful removal of cellular materials from native matrix while preserving most of ECM components. Different strategies, such as physical, mechanical, enzymatic, and chemical, results in different tissue morphological structures . SDS and Triton X based protocol are applicable for large volumes of native tissue samples [64]. In our study, efficiency of decellularization was increased by applying high concentration of SDS, which diffuses inside out of the organ model. This approach did not display any harmful effect on characteristic structure of tissue morphology and ECM structure. Maintenance of vascular and morphological structure is crucial for cellular attachment, homogeneous distribution of cell, and cellular proliferation before and after recellularization process. Additionally, preservation of vascular structure is essential for equivalent allocation of oxygen, nutrient, and glucose uptake via torsion testicular artery vessel in organ model. Characterization experiments of decellularized whole prostate matrix have showed that cells were efficiently removed by SDS-based protocol without damaging to tissue architecture and morphology. Prostate tissue morphology were maintained according to our histological assessments (Figure 3.4) [83-84]. Overall, tissue specific architecture, fiber formation, and porous structure for cell attachment were preserved with our optimized applied SDS-based decellularized procedure.

Extracellular matrix components regulate cellular events such as adhesion, differentiation, migration, proliferation, and survival [81]. ECM components in 3D cell culture model are required for *in vitro* cancer study. Extracellular matrix components in 3D cell culture models play essential role on progression and dissemination of tumor cells. In addition, 3D network of ECM structure and protein content in ECM directly affects on migration of tumor cells. Angiogenesis formation of tumor cells is also observed in 3D cell culture models. More than one hundred proteins were observed within the ECM itself. Effects of each extracellular matrix protein on cancer progression is under investigation in matrisome project. Distribution of ECM proteins are not only depends on organ type but internal organ structure. We have identified that immortalized prostate cell lines which were seeded inside decellularized prostate matrix significantly enhanced the expression of AHSG alpha 2-HS

glycoprotein (fetuin A) (Figure 3.6.). Fetuin-A functions in cancer cell invasion, motility, and attachment [85], [86]. Moreover, fetuin-A was thought to be a prognostic indicator for prostate cancer in the blood serums of patients [87]. On the other hand, adaptation of prostate cells in 3D cell culture environment and low glucose, nutrient, and oxygen levels in addition to different cell types or protein contents of ECM might result in the alteration of protein expression in decellularized prostate matrix (DPM). Gene expression of rat liver cells after recellularization of decellularized liver matrix showed different cluster on days 2, 15, and 28 [27]. However, our profiling of protein expressions on days 7, 15, 21 after recellularization of DPM did not display much difference on one dimensional SDS-polyacrylamide gel (Figure 3.9). Limitation of nutrient or serum in 3D cell culture model resulted also a similar proteomic profile (Figure 3.8). Then, cells were isolated from native matrix and from recellularized DPM. Intensity of high molecular weight proteins from recellularized DPM decreased compared to ones from native matrix (Figure 3.8)

Gel-based 3D matrix has been used as a scaffold for 3D cell culture for several years to mimic soft tissue environment. Different gel types and techniques were tested to provide more *in vivo* like tissue specific architecture and conditions. Matrigel is the most common gel-based biomaterial compared with other synthetic or natural sources. Home-made matrigel was used during recellularization process to increase recellularization efficiency and resulted in a similar proteome profile. Protein profile of cell lysate inside home-made matrigel displays comparable profile with native tissue lysate (Figure 3.10 (A)). Although matrigel contains only three extracellular matrix proteins, acellular matrices contain more than 100 different extracellular matrix proteins [88]. Then, different acellular matrices (mouse lung and liver) were tested as a 3D cell culture scaffold to obtain *in vitro* prostate cancer model. Recellularized liver matrix with prostate cells demonstrated more similar proteoin profile compared to recellularized and decellularized liver matrix, which was chosen as a model scaffold for our further *in vitro* prostate cancer studies (Figure 3.10 (B)). Proteome of 3D cell culture displays the changes between not only 3D and 2D cell culture but also before and after NaB treatment. Additionally, energy metabolism is directly affected from glucose and oxygen uptake in this system. Post-translational modifications (PTMs) regulate the activity of metabolic enzymes and also affect energy metabolism of cells. Acetylation is one of these post-translational modifications and controlled by sirtuins. Acetylation features on cellular processes such as cell survival and cellular energy state in cancerous cell. Sirtuins which are known as a NAD^+-dependent deacetylases or ADP ribosyl

transferases play part in cellular function such as inflammation, cell growth, circadian rhythm, energy metabolism, neuronal function, and stress resistance [60], [61]. Alteration of NAD^+/NADH level specifically regulates sirtuins, which are particularly activated under physiological stress conditions. Activity of sirtuins is also modulated in response to oxidative stress. 3D cell culture models restrict oxygen level inside the scaffold. Combination of NaB treatment along with calorie restriction activated sirtuins and restored mitochondrial function [45]. In this study, whole cell proteome, cellular acetylome, and expression of respiratory chain complexes were shown to be altered between 2D and 3D cell culture in addition to before and after NaB treatment (Figure 3.12. (A) and (B)).

In summary, we constructed a whole prostate organ culture with immortal prostate cancer cells (PNT1A, DU145, and PC3) and investigated the effect of boron on prostate cancer cell lines by comparing 2D versus 3D cell culture models such as acellular liver matrix and Matrigel models. Our results illustrated that expressed proteins of prostate cancer cell lines are affected from extracellular matrix proteins. To conclude, whole decellularized prostate matrix is not applicable for *in vitro* drug discovery research according to our results; while, liver matrix model with prostate cells can be utilized for cancer research studies to assess candidate drugs *in vitro* before *in vivo* stage.

5. CONCLUSION AND FUTURE PROSPECTS

This study showed that whole organ engineering system can be employed for *in vitro* drug discovery and cancer research studies before *in vivo* experiments. For this reason, similarities between *in vivo* and *in vitro* cell culture models need to be improved to obtain more accurate information about applications.

Different decellularization methods were tested for maximum retention of ECM components and for minimum cellular material residues. Each method was varied according to its application and materials for different organ types. However, cellular residues which cause immune responses, tissue rejection after transplantation, inflammation response, and adverse reactions of immunosuppressive regimens need to be eliminated. Proteomic analyses of non-ECM proteins content in whole organ is one of the most applicable strategies for the assessment of whole organ proteome.

Biomechanical and structural properties of native, decellularized, and recellularized tissue need to be characterized to optimize whole organ for physiological loading range. Loading range capability of each organ type must be tested before and after cancer cell progression within the sample organ. Assessment of vascular network (micro- and macro-vessels) and reendothelialization of whole organ might be analyzed with different approaches, for instance red blood cell hemolysis test, passing blood from disordered blood vessel, can be used as a marker in order to evaluate intactness of vascular network.

Real time monitoring of continuous prostate organ culture system and of physiological system provides more *in vivo* like system compared with traditional organ culture methods. Automated tracking of migration cells is another key factor to identify the distribution of cells inside whole organ. Combination of automated tracking system and continuous monitoring of cell migration would provide invaluable information during recellularization process. Cell heterogeneity inside whole organ is essential to mimic cell distribution in native tissue. Heterogeneity of cell population through histological analyses might be identified. Microfluidic chip along with integration of electrical cell impedance sensing (ECIS) in Boyden chamber design with microelectrode arrays is another strategy to analyze cancer cell migration inside organ during the whole process, which can be easily integrated in clinical application experiment model for *in vitro* drug and biological testing. In addition, nano-based prostate specific antigen (PSA) biosensor and tactile resonance sensor measuring

stiffness of glandular tissue with new bioreactor design might be accomplished to track cancer progression inside organ model. Overall, these systems would be more efficient for drug discovery field.

REFERENCES

1. Bray F, Ferlay J, Soerjomataram I, Siegel RL, Torre LA, Jemal A. Global cancer statistics 2018: GLOBOCAN estimates of incidence and mortality worldwide for 36 cancers in 185 countries. *CA Cancer Journal of Clinicians* 2018;68(6):394–424.
2. Bilhim T, Pisco JM, Furtado A, Casal D, Pais D, Pinheiro LC, et al. Prostatic arterial supply: demonstration by multirow detector angio CT and catheter angiography. *European Radiology* 2011;21(5):1119–26.
3. Aaron L, Franco O, Hayward SW. Review of prostate anatomy and embryology and the etiology of BPH. *Urology Clinics North America* 2016;43(3):279–88.
4. Strand DW, Goldstein AS. The many ways to make a luminal cell and a prostate cancer cell. *Endocrine Related Cancer* 2015;22(6):187–97.
5. Nagle RB, Ahmann FR, McDaniel KM, Paquin ML, Clark VA, Celniker A. Cytokeratin characterization of human prostatic carcinoma and its derived cell lines. *Cancer Research* 1987;47(1):281–6.
6. Verhagen AP, Aalders TW, Ramaekers FC, Debruyne FM, Schalken JA. Differential expression of keratins in the basal and luminal compartments of rat prostatic epithelium during degeneration and regeneration. *Prostate* 1988;13(1):25–38.
7. Yang Y, Hao J, Liu X, Dalkin B, Nagle RB. Differential expression of cytokeratin mRNA and protein in normal prostate, prostatic intraepithelial neoplasia, and invasive carcinoma. *American Journal of Pathology* 1997;150(1):693–704.
8. Josson S, Matsuoka Y, Chung LWK, Zhau HE, Wang R. Tumor-stroma co-evolution in prostate cancer progression and metastasis. *Seminars in Cell and Developmental Biology* 2010;21(1):26–32.
9. De Marzo AM, Marchi VL, Epstein JI, Nelson WG. Proliferative inflammatory atrophy of the prostate: implications for prostatic carcinogenesis. *American Journal of Pathology* 1999;155(6):1985–92.
10. De Marzo AM, Platz EA, Sutcliffe S, Xu J, Grönberg H, Drake CG, et al. Inflammation in prostate carcinogenesis. *Nature Review Cancer* 2007;7(4):256–69.
11. Graham MK, Meeker A. Telomeres and telomerase in prostate cancer development and therapy. *Nature Reviews Urology* 2017;14(10):607–19.

12. Rijal G, Bathula C, Li W. Application of synthetic polymeric scaffolds in breast cancer 3d tissue cultures and animal tumor models. *International Journal of Biomaterial* 2017;58(5):50-39.
13. Bružauskaitė I, Bironaitė D, Bagdonas E, Bernotienė E. Scaffolds and cells for tissue regeneration: different scaffold pore sizes—different cell effects. *Cytotechnology* 2016;68(3):355–69.
14. Ingber DE. *Comprehensive Physiology*, Hoboken: John Wiley and Sons, Inc.; 2011.
15. Bissell MJ, Rizki A, Mian IS. Tissue architecture: the ultimate regulator of breast epithelial function. *Current Opinion Cell Biology* 2003;15(6):753–62.
16. Hutchinson L, Kirk R. High drug attrition rates--where are we going wrong? *Nature Review Clinical Oncology* 2011;8(4):189–90.
17. Fennema E, Rivron N, Rouwkema J, van Blitterswijk C, de Boer J. Spheroid culture as a tool for creating 3D complex tissues. *Trends Biotechnology* 2013;31(2):108–15.
18. Pampaloni F, Reynaud EG, Stelzer EHK. The third dimension bridges the gap between cell culture and live tissue. *Nature Review Molecular Cell Biology* 2007;8(10):839–45.
19. Timmins NE, Harding FJ, Smart C, Brown MA, Nielsen LK. Method for the generation and cultivation of functional three-dimensional mammary constructs without exogenous extracellular matrix. *Cell Tissue Research* 2005;320(1):207–10.
20. Mehta G, Hsiao AY, Ingram M, Luker GD, Takayama S. Opportunities and challenges for use of tumor spheroids as models to test drug delivery and efficacy. *Journal of Control Release* 2012;164(2):192–204.
21. Kolb H-J. Graft-versus-leukemia effects of transplantation and donor lymphocytes. *Blood* 2008;112(12):4371–83.
22. Antoni D, Burckel H, Josset E, Noel G. Three-dimensional cell culture: a breakthrough in vivo. *International Journal of Molecular Science* 2015;16(3):5517–27.
23. Xia X, Li J, Xia B, Yang H, Zhang D, Zhou B, et al. Matrigel scaffold combined with Ad-hBMP7-transfected chondrocytes improves the repair of rabbit cartilage defect. *Experimental Therapeutic Medicine* 2017;13(2):542–50.
24. Hou S, Tiriac H, Sridharan BP, Scampavia L, Madoux F, Seldin J, et al. Advanced development of primary pancreatic organoid tumor models for high-throughput phenotypic drug screening. *SLAS Discovery* 2018;23(6):574–84.

25. Uygun BE, Soto-Gutierrez A, Yagi H, Izamis M-L, Guzzardi MA, Shulman C, et al. Organ reengineering through development of a transplantable recellularized liver graft using decellularized liver matrix. *Nature Medicine* 2010;16(7):814–20.
26. Sabetkish S, Kajbafzadeh A-M, Sabetkish N, Khorramirouz R, Akbarzadeh A, Seyedian SL, et al. Whole-organ tissue engineering: Decellularization and recellularization of three-dimensional matrix liver scaffolds. *Journal of Biomedical Materials Research Part A* 2015;103(4):1498–508.
27. Robertson MJ, Soibam B, O'Leary JG, Sampaio LC, Taylor DA. Recellularization of rat liver: An in vitro model for assessing human drug metabolism and liver biology. *PLoS ONE* 2018;13(1):0191892.
28. Wallis JM, Borg ZD, Daly AB, Deng B, Ballif BA, Allen GB, et al. Comparative assessment of detergent-based protocols for mouse lung de-cellularization and re-cellularization. *Tissue Engineering Part C Methods* 2012;18(6):420–32.
29. Devalliere J, Chen Y, Dooley K, Yarmush ML, Uygun BE. Improving functional re-endothelialization of acellular liver scaffold using REDV cell-binding domain. Acta *Biomaterialia* 2018;78(6):151–64.
30. Li Q, Uygun BE, Geerts S, Ozer S, Scalf M, Gilpin SE, et al. Proteomic analysis of naturally-sourced biological scaffolds. *Biomaterials* 2016;75(2):37–46.
31. Hill RC, Calle EA, Dzieciatkowska M, Niklason LE, Hansen KC. Quantification of extracellular matrix proteins from a rat lung scaffold to provide a molecular readout for tissue engineering. *Molecular Cellular Proteomics* 2015;14(4):961–73.
32. Vincent T, Mechti N. Extracellular matrix in bone marrow can mediate drug resistance in myeloma. *Leukemia and Lymphoma* 2005;46(6):803–11.
33. Demirtaş A. Bor'un insan beslenmesi ve sağlığı açısından önemi / Significance of boron for human nutrition and health. *Journal of the Faculty of Agriculture* 2010;41(1): 36-13.
34. Flores-Parra A, Contreras R. Boron coordination compounds derived from organic molecules of biological interest. *Coordination Chemistry Reviews* 2000;196(1):85–124.
35. Murray FJ. A comparative review of the pharmacokinetics of boric acid in rodents and humans. *Biological Trace Elem Research* 1998;66(1-3):331–41.
36. Park M, Li Q, Shcheynikov N, Muallem S, Zeng W. Borate transport and cell growth and proliferation. Not only in plants. *Cell Cycle* 2005;4(1):24–6.

37. Nzietchueng RM, Dousset B, Franck P, Benderdour M, Nabet P, Hess K. Mechanisms implicated in the effects of boron on wound healing. *J Trace Element Medical Biology* 2002;16(4):239–44.
38. Ameen HNM, Hussain SA, Ahmed ZA, Aziz TA. Anti-inflammatory effects of boron alone or as adjuvant with dexamethasone in animal models of chronic and granulomatous inflammation. *International Journal of Basic and Clinical Pharmacology* 2017;4(4):701–7.
39. Lee D, Park S, Bae S, Jeong D, Park M, Kang C, et al. Hydrogen peroxide-activatable antioxidant prodrug as a targeted therapeutic agent for ischemia-reperfusion injury. *Scientific Reports* 2015;5(2):16592.
40. Peng X, Gandhi V. ROS-activated anticancer prodrugs: a new strategy for tumor-specific damage. *Therapeutic Delivery* 2012;3(7):823–33.
41. Ince S, Kucukkurt I, Cigerci IH, Fatih Fidan A, Eryavuz A. The effects of dietary boric acid and borax supplementation on lipid peroxidation, antioxidant activity, and DNA damage in rats. *Journal of Trace Element and Medical Biology* 2010;24(3):161–4.
42. Cui Y, Winton MI, Zhang Z-F, Rainey C, Marshall J, De Kernion JB, et al. Dietary boron intake and prostate cancer risk. *Oncology Report* 2004;11(4):887–92.
43. Barranco WT, Eckhert CD. Cellular changes in boric acid-treated DU-145 prostate cancer cells. *British Journal of Cancer* 2006;94(6):884–90.
44. Henderson KA, Kobylewski SE, Yamada KE, Eckhert CD. Boric acid induces cytoplasmic stress granule formation, eIF2α phosphorylation, and ATF4 in prostate DU-145 cells. *Biometals* 2015;28(1):133–41.
45. Üstüner B, Çimen H. Sodium borate treatment induces metabolic reprogramming in hepatocellular carcinoma through SIRT3 activation. *Turkish Journal of Biology* 2016;40(2):906–14.
46. Suzuki H, Asakawa A, Amitani H, Fujitsuka N, Nakamura N, Inui A. Cancer cachexia pathophysiology and translational aspect of herbal medicine. *Japanese Journal of Clinical Oncology* 2013;43(7):695–705.
47. Marxsen JH, Stengel P, Doege K, Heikkinen P, Jokilehto T, Wagner T, et al. Hypoxia-inducible factor-1 (HIF-1) promotes its degradation by induction of HIF-alpha-prolyl-4-hydroxylases. *Biochemical Journal* 2004;381(3):761–7.
48. Zhang X, Qin Z, Wang J. The role of p53 in cell metabolism. *Acta Pharmacologica Sinica* 2010;31(9):1208–12.

49. Airley RE, Mobasheri A. Hypoxic regulation of glucose transport, anaerobic metabolism and angiogenesis in cancer: novel pathways and targets for anticancer therapeutics. *Chemotherapy* 2007;53(4):233–56.
50. Geschwind J-F, Georgiades CS, Ko YH, Pedersen PL. Recently elucidated energy catabolism pathways provide opportunities for novel treatments in hepatocellular carcinoma. *Expert Review of Anticancer Therapy* 2004;4(3):449–57.
51. Kim DH, Marbois BN, Faull KF, Eckhert CD. Esterification of borate with NAD+ and NADH as studied by electrospray ionization mass spectrometry and 11B NMR spectroscopy. *Journal of Mass Spectrometry* 2003;38(2):632–40.
52. Allfrey VG, Mirsky AE. Structural Modifications of Histones and their Possible Role in the Regulation of RNA Synthesis. *Science* 1964;144(3618):559.
53. Allis CD, Berger SL, Cote J, Dent S, Jenuwien T, Kouzarides T, et al. New nomenclature for chromatin-modifying enzymes. *Cell* 2007;131(4):633–6.
54. Kim J, Tchernyshyov I, Semenza GL, Dang CV. HIF-1-mediated expression of pyruvate dehydrogenase kinase: a metabolic switch required for cellular adaptation to hypoxia. *Cell Metabolism* 2006;3(3):177–85.
55. Koukourakis MI, Giatromanolaki A, Sivridis E, Bougioukas G, Didilis V, Gatter KC, et al. Lactate dehydrogenase-5 (LDH-5) overexpression in non-small-cell lung cancer tissues is linked to tumour hypoxia, angiogenic factor production and poor prognosis. *British Journal of Cancer* 2003;89(5):877–85.
56. Mazurek S, Boschek CB, Eigenbrodt E. The role of phosphometabolites in cell proliferation, energy metabolism, and tumor therapy. *Journal of Bioenergetics and Biomembranes* 1997;29(4):315–30.
57. Chen X, Qian Y, Wu S. The Warburg effect: evolving interpretations of an established concept. *Free Radical Biology and Medicine* 2015;79(14):253–63.
58. Hallows WC, Lee S, Denu JM. Sirtuins deacetylate and activate mammalian acetyl-CoA synthetases. *PNAS* 2006;103(27):10230–5.
59. Menzies KJ, Zhang H, Katsyuba E, Auwerx J. Protein acetylation in metabolism - metabolites and cofactors. *Nature Reviews Endocrinology* 2016;12(1):43–60.
60. Guo X, Kesimer M, Tolun G, Zheng X, Xu Q, Lu J, et al. The NAD^+-dependent protein deacetylase activity of SIRT1 is regulated by its oligomeric status. *Scientific Reports* 2012;2(1):00640.

61. Morris BJ. Seven sirtuins for seven deadly diseases of aging. *Free Radical Biology and Medicine* 2013;56(1):133–71.
62. Lombard DB, Tishkoff DX, Bao J. Mitochondrial sirtuins in the regulation of mitochondrial activity and metabolic adaptation. *Handbook of Experimental Pharmacology* 2011;206(8):163–88.
63. Kumar S, Lombard DB. Mitochondrial sirtuins and their relationships with metabolic disease and cancer. *Antioxidants and Redox Signaling* 2015;22(12):1060–77.
64. Newman JC, He W, Verdin E. Mitochondrial protein acylation and intermediary metabolism: regulation by sirtuins and implications for metabolic disease. *The Journal of Biological Chemistry* 2012;287(51):42436–43.
65. Neuzil J, Dong L-F, Rohlena J, Truksa J, Ralph SJ. Classification of mitocans, anti-cancer drugs acting on mitochondria. *Mitochondrion* 2013;13(3):199–208.
66. Vaupel P, Mayer A. Availability, not respiratory capacity governs oxygen consumption of solid tumors. *The International Journal of Biochemistry and Cell Biology* 2012;44(9):1477–81.
67. Vaitheesvaran B, Xu J, Yee J, Q-Y L, Go VL, Xiao GG, et al. The Warburg effect: a balance of flux analysis. *Metabolomics* 2015;11(4):787–96.
68. Shibanuma M, Kuroki T, Nose K. Superoxide as a signal for increase in intracellular pH. *Journal of Cellular Physiology* 1988;136(2):379–83.
69. Breedveld P, Zelcer N, Pluim D, Sönmezer O, Tibben MM, Beijnen JH, et al. Mechanism of the pharmacokinetic interaction between methotrexate and benzimidazoles: potential role for breast cancer resistance protein in clinical drug-drug interactions. *Cancer Research* 2004;64(16):5804–11.
70. Cardone RA, Casavola V, Reshkin SJ. The role of disturbed pH dynamics and the Na+/H+ exchanger in metastasis. *Nature Review Cancer* 2005;5(10):786–95.
71. Diaz-Moralli S, Tarrado-Castellarnau M, Miranda A, Cascante M. Targeting cell cycle regulation in cancer therapy. *Pharmacology and Therapy* 2013;138(2):255–71.
72. White KA, Grillo-Hill BK, Barber DL. Cancer cell behaviors mediated by dysregulated pH dynamics at a glance. *Journal of Cell Science* 2017;130(4):663–9.
73. Verdin E, Hirschey MD, Finley LWS, Haigis MC. Sirtuin regulation of mitochondria: energy production, apoptosis, and signaling. *Trends in Biochemical Sciences* 2010;35(12):669–75.

74. Kim JB. Three-dimensional tissue culture models in cancer biology. *Seminars Cancer Biology* 2005;15(5):365–77.
75. Galina A. Mitochondria: 3-bromopyruvate vs. mitochondria? A small molecule that attacks tumors by targeting their bioenergetic diversity. *International Journal of Biochemistry and Cell Biology* 2014;54(1):266–71.
76. Cheng G, Zielonka J, McAllister D, Hardy M, Ouari O, Joseph J, et al. Antiproliferative effects of mitochondria-targeted cationic antioxidants and analogs: Role of mitochondrial bioenergetics and energy-sensing mechanism. *Cancer Letters* 2015;365(1):96–106.
77. Li X, Jiang Y, Meisenhelder J, Yang W, Hawke DH, Zheng Y, et al. Mitochondria-translocated pgk1 functions as a protein kinase to coordinate glycolysis and the tca cycle in tumorigenesis. *Molecular Cell* 2016;61(5):705–19.
78. Branco AF, Ferreira A, Simões RF, Magalhães-Novais S, Zehowski C, Cope E, et al. Ketogenic diets: from cancer to mitochondrial diseases and beyond. *European Journal of Clinical Investigation* 2016;46(3):285–98.
79. Buono R, Longo VD. Starvation, Stress Resistance, and Cancer. *Trends in Endocrinology and Metabolism* 2018;29(4):271–80.
80. Anderson KA, Madsen AS, Olsen CA, Hirschey MD. Metabolic control by sirtuins and other enzymes that sense NAD+, NADH, or their ratio. *Biochimica et Biophysica Acta Bioenergineering* 2017;1858(12):991–8.
81. Bissell MJ, Kenny PA, Radisky DC. Microenvironmental regulators of tissue structure and function also regulate tumor induction and progression: the role of extracellular matrix and its degrading enzymes. *Cold Spring Harbor Symposia Quantitative Biology* 2005;70(1):343–56.
82. Sainio A, Järveläinen H. Extracellular matrix macromolecules: potential tools and targets in cancer gene therapy. *Molecular and Cellular Therapies* 2014;2(1):4.
83. Cebotari S, Tudorache I, Jaekel T, Hilfiker A, Dorfman S, Ternes W, et al. Detergent decellularization of heart valves for tissue engineering: toxicological effects of residual detergents on human endothelial cells. *Artificial Organs* 2010;34(3):206–10.
84. Xu K, Kuntz LA, Foehr P, Kuempel K, Wagner A, Tuebel J, et al. Efficient decellularization for tissue engineering of the tendon-bone interface with preservation of biomechanics. *PLOS ONE* 2017;12(2):0171577.

85. Nangami GN, Sakwe AM, Izban MG, Rana T, Lammers PE, Thomas P, et al. Fetuin-A (alpha 2HS glycoprotein) modulates growth, motility, invasion, and senescence in high-grade astrocytomas. *Cancer Medicine* 2016;5(12):3532–43.
86. Nangami G, Koumangoye R, Shawn Goodwin J, Sakwe AM, Marshall D, Higginbotham J, et al. Fetuin-A associates with histones intracellularly and shuttles them to exosomes to promote focal adhesion assembly resulting in rapid adhesion and spreading in breast carcinoma cells. *Experimental Cell Research* 2014;328(2):388–400.
87. Mintz PJ, Rietz AC, Cardó-Vila M, Ozawa MG, Dondossola E, Do K-A, et al. Discovery and horizontal follow-up of an autoantibody signature in human prostate cancer. *Proceedings of the National Academy of Sciences USA* 2015;112(8):2515–20.
88. Naba A, Clauser KR, Hoersch S, Liu H, Carr SA, Hynes RO. The matrisome: in silico definition and in vivo characterization by proteomics of normal and tumor extracellular matrices. *Molecular and Cellular Proteomics* 2012;11(4):14647-13.